Theory and algorithms to compute Helfrich bending forces: A review

Achim Guckenberger* and Stephan Gekle
Biofluid Simulation and Modeling, Fachbereich Physik, Universität Bayreuth
(Dated: February 24, 2017)

Cell membranes are vital to shield a cell's interior from the environment. At the same time they determine to a large extent the cell's mechanical resistance to external forces. In recent years there has been considerable interest in the accurate computational modeling of such membranes, driven mainly by the amazing variety of shapes that red blood cells and model systems such as vesicles can assume in external flows. Given that the typical height of a membrane is only a few nanometers while the surface of the cell extends over many micrometers, physical modeling approaches mostly consider the interface as a two-dimensional elastic continuum.

Here we review recent modeling efforts focusing on one of the computationally most intricate components, namely the membrane's bending resistance. We start with a short background on the most widely used bending model due to Helfrich. While the Helfrich bending energy by itself is an extremely simple model equation, the computation of the resulting forces is far from trivial. At the heart of these difficulties lies the fact that the forces involve second order derivatives of the local surface curvature which by itself is the second derivative of the membrane geometry. We systematically derive and compare the different routes to obtain bending forces from the Helfrich energy, namely the variational approach and the thin-shell theory. While both routes lead to mathematically identical expressions, so-called linear bending models are shown to reproduce only the leading order term while higher orders differ. The main part of the review contains a description of various computational strategies which we classify into three categories: the *force*, the *strong* and the *weak* formulation. We finally give some examples for the application of these strategies in actual simulations.

Keywords: Helfrich bending, simulations, thin shell theory, variational derivative, red blood cells, vesicles, capsules, elastic membranes, spherical harmonics, subdivision surface methods, triangulated meshes

CONTENTS

* Corresponding author; achim.guckenberger@uni-bayreuth.de

I. INTRODUCTION

When immersed into an external flow, even such simple soft objects as vesicles or red blood cells (RBCs) deform into an amazing variety of dynamically moving shapes including slippers, parachutes or tumbling discocytes [1–5]. These arise from the complex interplay between the external and internal flow and the mechanical stiffness of the membrane. In the case of red blood cells the membrane consists of four components [6, 7]: shear resistance due to the network of cross-linked spectrin proteins (cytoskeleton) and bending rigidity as well as area inextensibility and surface viscosity due to the lipid bilayer. Omitting the lipid bilayer leads to objects which have no or very little bending resistance and which are commonly denoted as capsules [5]. Removal of the spectrin network eliminates shear resistance leading to what is called a vesicle [4]. For theoretical or computational modeling, membranes are typically considered as two-dimensional elastic sheets and their physical complexity is lumped into effective moduli for shear resistance, bending rigidity, area dilatation and sometimes surface viscosity [2, 8].

The study of soft object dynamics in flows is a serious challenge. Being deprived of a minimum energy principle in this non-equilibrium situation, the analytical prediction of cell and vesicle dynamics represents a formidable task. Experimentally, a full appreciation of the dynamics would require three-dimensional recordings combined with time-resolved tracking of the membrane while usually one is restricted to two-dimensional microscopic imaging. Although considerable progress has been achieved to overcome these theoretical [2, 9] and experimental [10–14] difficulties, in many situations one currently depends on numerical simulations to gain further insight into the physical phenomena and mechanisms governing the objects' behavior in external flows. An accordingly large interest exists in the development and validation of accurate and efficient numerical techniques [1, 8, 15–20].

In this review, we focus on one specific aspect of these numerical simulations, namely the bending forces originating from the lipid bilayer. Bending forces are important for the accurate modeling of vesicles, red blood cells and sometimes even capsules [1, 4, 5]. The typical starting point for their computation is an energy functional that provides the bending energy density for a given membrane geometry. In its most simple and, at the same time, most commonly used form the local bending energy density is proportional to the square of the local surface curvature. Variants of this form have been postulated by Canham [21], Helfrich [22] and Evans [23] in the early 1970s, but can also be derived from classical elasticity or by taking the continuum limit of models that explicitly consider the interaction between individual lipid molecules. In the mathematics community the bending functional is known under the term "Willmore surface/energy" [24–26].

Our goal is to summarize the origins of this energy, to outline different derivations of the ensuing bending forces and finally to give an account of available numerical algorithms together with an overview of recent applications. A detailed assessment of the quality of a variety of methods can be found in two recent papers [27, 28]. We do not cover other aspects such as shear elasticity or flow solvers. For these we refer the reader to recent reviews [8, 15, 17, 19] and books [16, 29]. Other related reviews [2, 4, 5, 18, 30] also include experimental observations. Collective behavior of many soft objects with a focus on blood flow is reviewed in references [20, 31–33].

The organization of the paper is as follows. In section II A we introduce the physical motivation of the Helfrich bending energy and outline how to derive the bending forces via a variational derivative as well as thin shell theory. The latter is given in detail in appendix A, which allows us to draw a connection to so-called "linear bending models". In sections II B and II C we briefly touch upon the still open question of the spontaneous curvature and introduce some experimental techniques to measure the bending modulus. Section III A discusses various possibilities to represent the membrane shape in a discretized fashion for use in computer algorithms. Based on these, section III B focuses on a classification of different computational methods according to their conceptual similarities and differences. In section III C we briefly summarize results of a recent comparison regarding the quality of different algorithms [27] and extend the comparison to the important case of spherical harmonics, with details provided in appendix B. Finally, in section IV we describe some recent applications of the computational algorithms.

II. PHYSICAL MODEL OF MEMBRANE BENDING

A. The Helfrich model

1. *Bending energy*

Vesicle walls and red blood cell membranes contain a lipid bilayer which leads to the membrane's resistance against bending as well as its rather strict area inextensibility [4, 6, 7]. The bilayer consists of two neighboring sheets of elongated lipid molecules whose axes are oriented perpendicular to the membrane surface. Their hydrophilic heads point outwards towards the aqueous surrounding while the hydrophobic tails are buried in the membrane interior. Different forms of the bending energy have been proposed in the past, with the common denominator that they all depend on the square of the mean curvature [21–24]. One of the most popular models for the energy per unit deformed area ϵ_B dates back to Helfrich [22], who

introduced it as

$$\epsilon_{\mathrm{B}}(\boldsymbol{x}) = 2\kappa_{\mathrm{B}}\left(H - H_0\right)^2 + \kappa_{\mathrm{K}} K\,, \quad \boldsymbol{x} \in S\,. \tag{1}$$

This constitutive law has later been called the spontaneous curvature model [34], also compare section II B. All appearing quantities might in principle depend on $\boldsymbol{x}$. The total bending energy stored in the infinitesimally thin interface S is then

$$E_{\mathrm{B}} = \int_S 2\kappa_{\mathrm{B}}\left(H - H_0\right)^2 \mathrm{d}S + \int_S \kappa_{\mathrm{K}} K \mathrm{d}S\,. \tag{2}$$

Here, κ_{B} is the usually constant bending modulus (having unit of energy) and $H(\boldsymbol{x})$ is the local mean curvature which is defined by

$$H(\boldsymbol{x}) = \frac{1}{2}\left(\kappa_1 + \kappa_2\right)\,, \quad \boldsymbol{x} \in S\,, \tag{3}$$

i.e. the average of the principal curvatures κ_1 and κ_2 [35, 36]. Note that the sign of H can be defined such that it is either positive or negative for a sphere. We adopt the convention that H shall be positive for a sphere. An alternative but equivalent expression is given by [37]

$$H(\boldsymbol{x}) = \frac{1}{2}\sum_{i=1}^{3}\left(\Delta_{\mathrm{S}} x_i\right) n_i(\boldsymbol{x})\,, \quad \boldsymbol{x} \in S\,, \tag{4}$$

where $\boldsymbol{n}$ is the outer normalized normal vector and Δ_{S} is the so-called Laplace-Beltrami operator [36, eq. (33)]. This form reveals more clearly that the bending energy already involves a second order derivative of the surface. This can be contrasted with the surface tension of a liquid-liquid interface whose energy involves only the area itself.

The Gaussian curvature is $K(\boldsymbol{x}) = \kappa_1\kappa_2$ and its associated Gaussian (or saddle splay) modulus is κ_{K}. Both moduli κ_{B} and κ_{K} are often similar in magnitude [36]. However, the Gauss-Bonnet theorem [36, eq. (70)] states that the integral of K over a closed (but not an open [36, 38–42]) surface is a topological invariant, i.e. it is a constant as long as the topology for a closed object does not change. Hence, it can often be discarded from the very beginning. H_0 is the spontaneous curvature which will be discussed further in section II B below. We point the reader to reference [36] for an excellent overview of the required math and the Helfrich Hamiltonian in general.

Equation (1) can be obtained via three different routes. In the original work [22] the form of the energy functional (1) has been phenomenologically proposed. It can also be justified by the observation that the energy density for fluid membranes can only depend on the local area stretch and the mean and Gaussian curvatures. Taylor expansion to second order then leads to an expression of the form (1) [36, 43, 44]. In light of this it is somewhat surprising that it remains valid even when $1/H$ is of the same order of magnitude as the bilayer thickness [45].

Secondly, eq. (1) can also be derived from a continuum mechanics perspective.[1] Here, one starts by considering the membrane as a three-dimensional isotropic and linear (i.e. Hookean) elastic material. In the limit of thin and inextensible shells, a careful derivation of the elastic stresses and the resulting elastic energy for a given deformation then leads to an expression equivalent to the first and most important term in eq. (1) (compare [44, eq. (24)] [46, eq. (1.132)] [35, eq. (4.52)] [48, eq. (7)]). The bending modulus κ_{B} can then be calculated explicitly as a function of the membrane thickness h and the elastic parameters (e.g. Young's modulus E) of the material [5, 36, 44, 48]. Given the complex molecular structure of RBCs [6], the assumption of isotropic and homogeneous elastic properties of the lipid bilayer may however be called into question for cells and an empirical approach to the value of κ_{B} might be a better choice.

In the third method, the form of eq. (1) is derived from microscopic models that consider individual lipid molecules. Assuming an interaction potential between the molecules and taking the limit of an infinite amount of molecules, one arrives at eq. (1) [49, 50]. Molecular scale models can be combined with the continuum mechanics approach given in the previous paragraph by assuming spatial variability of the elastic parameters [51] which to lowest order again leads to equation (1).

2. *Bending forces*

The term "bending force" in the present context needs to be understood in the following way: Consider a deformed membrane S whose shape is known. The deformation results in forces $\boldsymbol{f}_{\mathrm{B}}(\boldsymbol{x})$ driving the interface back to equilibrium. At the same time, flows on the outside and inside of the membrane result in tractions (forces per unit area), whose difference across the surface provides a traction jump $\triangle\boldsymbol{f}_{\mathrm{B}}(\boldsymbol{x})$. Assuming negligible membrane inertia, the internal membrane bending forces must be in local equilibrium with the external fluid traction jump at each point in time, implying [5, 35, 52]

$$\triangle\boldsymbol{f}_{\mathrm{B}}(\boldsymbol{x}) = -\boldsymbol{f}_{\mathrm{B}}(\boldsymbol{x})\,, \quad \boldsymbol{x} \in S\,. \tag{5}$$

The goal now is to compute the bending forces $\boldsymbol{f}_{\mathrm{B}}$ or equivalently the traction jump $\triangle\boldsymbol{f}_{\mathrm{B}}$ from the current deformation if the energy stored in the surface is given by equation (2). Analytically, this goal is commonly achieved by one of two possibilities.

a. Variational formulation In the first approach one performs a variational derivative of eq. (2) while applying some external force such that the membrane is in equilibrium. Consider arbitrary infinitesimal and virtual displacements $\delta\boldsymbol{x}$ (but which adhere to possible constraints)

[1] Note that in engineering solid mechanics the term "membrane theory" actually refers to thin shells *without* bending resistance [46, 47].

of the vector $\boldsymbol{x}$ that maps the deformed surface. The virtual work performed by the forces when some membrane point is displaced is thus given by $\triangle \boldsymbol{f}_\mathrm{B} \cdot \delta\boldsymbol{x}$, and for the whole membrane by $\delta W_\mathrm{ext} := \int_S \triangle \boldsymbol{f}_\mathrm{B}(\boldsymbol{x}) \cdot \delta\boldsymbol{x}\, \mathrm{d}S(\boldsymbol{x})$. Hence, the membrane is in equilibrium for [53–57]

$$\begin{aligned} \delta\mathcal{E} &:= \delta E_\mathrm{B} - \delta W_\mathrm{ext} \\ &= \delta E_\mathrm{B} - \int_S \triangle \boldsymbol{f}_\mathrm{B}(\boldsymbol{x}) \cdot \delta\boldsymbol{x}\, \mathrm{d}S(\boldsymbol{x}) \stackrel{!}{=} 0\,. \end{aligned} \tag{6}$$

Explicitly evaluating δE_B from eq. (2) for variations in the normal direction and evoking the arbitrariness of $\delta\boldsymbol{x}$ eventually leads to the Euler-Lagrange equation [24, 36, 41, 57–66]

$$\begin{aligned} \triangle \boldsymbol{f}_\mathrm{B} = -2\kappa_\mathrm{B}[&\Delta_\mathrm{S}\,(H - H_0) \\ &+ 2\,(H - H_0)\,(H^2 - K + H_0 H)]\boldsymbol{n}\,. \end{aligned} \tag{7}$$

H_0, H, K and $\boldsymbol{n}$ may depend on the position $\boldsymbol{x} \in S$. κ_B and κ_K, on the other hand, are assumed to be constant. If they were not, an additional tangential term would arise [67]. Note that for constant moduli without additional constraints and for closed objects tangential variations only represent a reparameterization of the surface and provide no further information [61], i.e. the traction jump consists of only the above normal component.

Equation (7) and variations thereof can be used to determine the equilibrium shapes of vesicles for $\triangle \boldsymbol{f}_\mathrm{B} = 0$ [17, 21, 34, 58, 68–70]. In the context of hydrodynamic simulations, the reverse problem is considered and the traction jump $\triangle \boldsymbol{f}_\mathrm{B}$ is determined from the instantaneous deformation. $\triangle \boldsymbol{f}_\mathrm{B}$ is exerted by the fluid on the membrane and is the central quantity which couples the solid and the fluid mechanics part of the problem [35, 71, 72]. Explicit expressions for the stress tensor also exist (eq. (A43) in the appendix), representing a first integral of equation (7) [2, 36, 57, 61, 65, 70, 73].

Note that the Euler-Lagrange equation (7) also remains valid if the surface is not closed: The first normal variation of the second term in eq. (2) that contains the (constant) saddle splay modulus κ_K still drops out [36, 38, 41]. Yet, contrary to the case of closed objects without constraints, demanding that the first *tangential* variation of $\mathcal{E}$ vanishes now provides additional information, namely boundary conditions for the shape at the borders that actually do depend on κ_K [38–40, 74]. I.e. although equation (7) remains valid in the interior of the surface, additional conditions arise at the borders that determine the possible shapes in agreement with recent experiments on vesicles [42].

b. Shell formulation The second approach to derive eq. (7) uses thin shell theory [35, 70, 75–78]. Tension tensor and bending moments can be obtained by computing appropriate derivatives of the energy density with respect to the metric and curvature tensors, respectively. Balancing these by the externally imposed traction jump $\triangle \boldsymbol{f}_\mathrm{B}$ invokes first a local torque and subsequently a local force balance. Yet, in the end eq. (7) is obtained [76, eq. (6.19)]. We explicitly perform this calculation and show the equivalence of the two approaches in appendix A.

c. Linear bending models Sometimes one directly starts with a constitutive linear model [70, 79–82] for the bending moments $M_{\alpha\beta}$ on S, such as

$$M_{\alpha\beta} = -2\kappa_\mathrm{B}(H - H_0)a_{\alpha\beta}\,, \quad \alpha, \beta = 1, 2\,, \tag{8}$$

where $a_{\alpha\beta}$ is the metric tensor (the coefficients of the first fundamental form) and Greek indices denote curvilinear components. This ansatz leads to equation (7) only if additional contributions to the tension tensor are appropriately accounted for. However, deviant forms of eq. (8) (often involving the curvature tensor [54, 80, 81, 83–86]) and/or neglecting the tension tensor contributions are commonly used and usually yield only the leading order term ($\Delta_\mathrm{S} H$) from equation (7) when considering small deviations from a plane as shown in appendix A 5. Higher orders may differ [48, 58, 79]. Since the relations between these various approaches are not clearly established in the present literature, we derive and compare the traction jumps for these models in some detail in appendix A 5.

d. Constraints Many derivations of eq. (7) enforce additional constraints, such as constant volume (for closed particles) or conserved surface area which mimic the balance of osmotic pressure and the large area dilatation modulus, respectively, of vesicles [4, 34] and red blood cells [1, 6, 87]. These lead to additional terms containing Lagrange multipliers that are added to $\mathcal{E}$ and also modify the Euler-Lagrange equation. For the volume conservation, $\mathcal{E}$ is complemented by $\triangle p\, V$, where V is the particle's volume and the Lagrange multiplier $\triangle p$ represents a pressure difference [39, 41, 59–61, 64]. Equation (7) receives an additional $\triangle p\, \boldsymbol{n}$.

Furthermore, two possibilities exist to enforce a constant surface area: either a local or a total area constraint. The total surface area constraint is implemented by adding $\sigma \int_S \mathrm{d}S$ to $\mathcal{E}$, with the Lagrange multiplier σ being a constant effective tension [36, 38, 39, 59, 60, 64, 88]. This leads to the supplement $2\sigma H \boldsymbol{n}$ in equation (7).

The local surface area constraint, on the other hand, is enforced by adding $\int \tilde{\sigma}(\boldsymbol{x})\mathrm{d}S$ to $\mathcal{E}$, where the Lagrange multiplier $\tilde{\sigma}(\boldsymbol{x})$ is a non-constant effective tension [2, 13, 52, 55, 58, 61, 88–99]. A *tangential* first variation of the total energy $\mathcal{E}$ then leads to an equation involving $\tilde{\sigma}$, whereas the normal first variation gives the Euler-Lagrange equation. Combining both effectively means to amend eq. (7) with the term $2\tilde{\sigma} H \boldsymbol{n} - \boldsymbol{\nabla}_\mathrm{S}\tilde{\sigma}$, where $\boldsymbol{\nabla}_\mathrm{S}$ denotes the surface gradient [52, eq. (60)]. We explicitly derive this term in section A 6. Now, if one solves the Euler-Lagrange equation for the shape, $\tilde{\sigma}$ is fixed by the tangential equation. Since we prescribe the surface and solve for $\triangle \boldsymbol{f}_\mathrm{B}$, $\tilde{\sigma}$ is determined from the incompressibility of the lipid bilayer fluid flow, $\boldsymbol{\nabla}_\mathrm{S} \cdot \boldsymbol{u} = 0$ [52]. This is equivalent to stipulating that the area of a small surface patch should remain constant [100, ch. 1.7.2]. We also note that $\tilde{\sigma}$ must be necessarily constant for closed objects without external forces, meaning that both the local and global models often predict the same equilibrium behavior [41, 55].

Directly solving for the Lagrange multipliers is possible [52, 77, 88, 92, 101–103]. For simplicity, constraints are also often implemented approximately using penalty methods. For example, one may introduce appropriate *ad-hoc* potential energies to penalize deviations from the desired values [55, 72, 93, 104–107]. In the case of area inextensibility it is also possible to use suitable in-plane elasticity models (such as the Skalak constitutive law [108]) to replace [94, 109] or supplement [72, 110] other area constraints.

e. Membrane inertia Equation (5) implies that the fluid and the membrane are always in local equilibrium. This means that the inertia of the membrane itself is neglected (otherwise an additional acceleration term would appear [78, 111, 112]). This is common even for those methods where the *fluid* inertia is included such as Lattice-Boltzmann [72, 113]. Thus, the motion of the membrane is determined by the no-slip condition, i.e. the local membrane velocity is taken equal to the local fluid velocity.

An alternative approach is to endow the membrane itself with a mass and to obtain its motion by integration of Newton's third law (force formulation, see III B 2) which is common practice in particle methods such as multiparticle collision dynamics (MPCD) [114–116] or (smoothed) dissipative particle dynamics [18, 117–126].

f. Finite thickness and other models Some simulations incorporate a membrane with a finite thickness. This effectively means to drop some simplifying assumptions that ultimately lead to the Helfrich model [127–133]. Explicitly taking into account the two leaflets for bilayer membranes has also been done [134]. Finally, ad-hoc models are sometimes used that have no (or at least no obvious) connection to the Helfrich law [135–137].

B. Area-difference model and spontaneous curvature

In many situations, especially for closed objects such as cells [6] or vesicles [34], the two sheets composing the lipid bilayer are not identical. For example, the inner layer may possess less or different lipids than the outer one. The minimum energy state is then no longer a flat sheet, but a curved shape with a prescribed difference $\triangle A_0$ between the areas occupied by the two sheets. Such a situation can be modeled by including an additional contribution to the energy in eq. (2), leading to the area-difference elasticity (ADE) model [34, 70, 138–140]:

$$E_\mathrm{B} = \int_S \epsilon_\mathrm{B}\,\mathrm{d}S + \kappa_\triangle \left(\triangle A - \triangle A_0\right)^2 . \tag{9}$$

$\kappa_\triangle$ is the area difference elastic modulus and $\triangle A$ is the instantaneous area difference expressible by the distance h between the neutral surfaces of the lipid monolayers as $\triangle A = 2h \int_S H\,\mathrm{d}S$ [36, eq. (77)]. For $\kappa_\triangle \to \infty$ the area difference becomes a hard constraint and the so-called bilayer coupling model is obtained [34, 138, 141]. The contributions of H, H_0, $\triangle A$ and $\triangle A_0$ to the traction jump differ from each other in general, i.e. cannot be merged. Nevertheless, when solving for the stationary shapes, the *total set* of solutions is the same when using either H_0 or $\kappa_\triangle$ or both [138, 142]. Yet, the full ADE model has apparently not been used to study soft objects in flows where the instantaneous shape is given as input, with the exception of reference [143]. This might therefore be a promising task for the future, but for the remainder of this paper we will restrict ourselves to H_0, i.e. to the Helfrich model (1).

A slightly more complicated situation arises when molecules other than lipids, e.g. transmembrane proteins, are present in the bilayer. These usually extend across both monolayers and may occupy a different area at one end than at the other, resulting again in an area difference. However, in contrast to a simple difference in the number of lipids, membrane proteins can often form clusters and/or are chemically attached to other parts of the cell membrane such as the spectrin network [6], leading to a spatially inhomogeneous spontaneous curvature $H_0(\boldsymbol{x})$.

While it is possible to obtain experimental values for H_0 for vesicles [56, 144], there currently exist no direct measurements of the spontaneous curvature (or area difference) of red blood cells, although the asymmetric distribution of the phospholipid types between the two leaflets of the bilayer [6] suggests a non-zero spontaneous curvature. Indeed, not even the stress-free shape for the in-plane shear elasticity could be determined unambiguously so far [145–147]. All in all, this lack of knowledge represents a certain hindrance to accurate red blood cell simulations. Different ways to overcome it have been suggested [66, 82, 139], although a consensus has yet to be reached.

The area-difference and bilayer-coupling models have been extensively used to compute vesicle equilibrium shapes (see section IV A). For cells or vesicles in external flows, the spontaneous curvature model following eq. (1) is more popular and most (but not all) numerical algorithms for bending forces described in the following section can relatively easily incorporate an arbitrary $H_0(\boldsymbol{x})$. Due to the experimental uncertainty, however, many red blood cell simulations are conducted with $H_0 = 0$. Yet, some researchers [82, 109, 148] choose a constant $H_0 \neq 0$ while others [72, 84, 85, 149] set $H_0(\boldsymbol{x}) = H_\mathrm{R}(\boldsymbol{x})$ where $H_\mathrm{R}(\boldsymbol{x})$ is the curvature of the resting shape, i.e. the shape that the object assumes in the absence of any external forces or flows. For red blood cells $H_\mathrm{R}(\boldsymbol{x})$ corresponds to the discocyte shape (cf. fig. 2). A recent careful analysis [66] suggested the spontaneous curvature of an oblate spheroid as a viable alternative for red blood cells.

C. Experimental determination of bending moduli

The bending modulus κ_B is a simulation parameter which needs to be determined by experiments. Various experimental setups exist for this task (see e.g. the reviews [144, 150–152] for vesicles and [7, 153] for red blood cells). Each experimental setup can be modeled either

analytically or numerically with κ_B as a free parameter whose value is then adjusted until agreement between the model and the experimental data is obtained.

In the first and most classical approach for cells, the membrane is sucked into a micropipette while the shape is recorded with a microscope as a function of the pressure difference [154–157]. The deformed shape sensitively depends on the elastic parameters of the cell and can be used to determine the bending modulus κ_B. Besides that, the shapes obtained by micropipette aspiration simulations can be directly compared to experiments which serves as a validation for the entire RBC model including, but not limited to, the bending algorithm [158, 159].

Secondly, the bending modulus can be computed from the wavelength of wrinkles at low flow strength as has been done for elastic capsules [131, 160], but has also been proposed for lipid membranes [161, 162].

Finally, the fluctuations of the cell membrane in thermal equilibrium (e.g. [163–168]) can be used to measure the bending modulus or to validate simulation models [105], although some complications may arise due to active processes in the cell membrane [169].

In principle, the above techniques can also be used to retrieve the bending modulus from molecular dynamics simulations. This has indeed been done for vesicles (see e.g. [45, 152, 170–173]), but apparently no one has attempted it so far for realistic RBCs.

The popular approach to measure elasticity constants by the stretching of cells via tweezers [174, 175] or atomic force microscopes [176] is unfortunately rather insensitive to the bending rigidity and can consequently not be used to obtain accurate information about that particular component [66, fig. 6] [105]. Nevertheless, these experiments have often been used to validate other parts of computational models [66, 105, 107, 135, 177–182].

In the end, measured values for κ_B of healthy human red blood cells scatter rather widely in the range of $0.2 - 9 \times 10^{-19}$ J [8, 153, 155]. Most simulations are being conducted with values between 2 and 4×10^{-19} J.

III. NUMERICAL APPROACHES

A. Surface discretizations

As already noted in the previous sections, cells, capsules and vesicles are typically modeled with infinitely thin surfaces. The finite (albeit very small) thickness is effectively taken into account via constitutive laws, for example the Helfrich model from equation (1). Such 2D manifolds embedded into the 3D space are usually implemented numerically by representing the surface with a distribution of points (nodes). Integration and differentiation operations are then calculated via some interpolation or approximation of the surface between these nodes. These discretizations form the basis for the computation of bending forces and we therefore describe some commonly used approaches in the following:

a. Flat triangles The simplest method uses linear interpolation between 3 nodes together with an unstructured mesh, leading to a representation with flat triangles. It is one of the most often used approaches owing to its simplicity and versatility ([52, 71, 93, 94, 98, 107, 183] among many others). For example, a local increase of resolution (refinement) is easily possible and was used in the biofluidic context e.g. in references [15, 110, 184–186] (see ref. [187] for a recent overview of refinement methodologies). However, since it leads to a $\mathcal{C}^0$ surface, computation of higher derivatives such as curvatures even within the elements requires the inclusion of several neighbors. Moreover, the results are often sensitive to the mesh regularity [27].

Spring network models [17, 18, 105, 135, 136, 158, 177, 188, 189] can also be classified into this category (although one could imagine spring networks containing quadrilaterals and other elements in principle, in practice they appear to be only used with triangles).[2] The major difference between these models and the continuum models emerges in the computation of in-plane elasticities [191], where their merit lies in the simplicity of implementation. Expressions for the bending resistance, on the other hand, usually assume the same form as in the continuum descriptions and follow the same methodologies as in the "force formulation" (see section III B 2 below).

b. Higher order elements Quadratic interpolation between 6 nodes leads to curved triangles [54, 71, 83, 192, 193]. They have the advantage that second order properties (such as the curvatures) within an element can be computed by direct differentiation. Nevertheless, even first order derivatives at the nodes or element borders remain ambiguous, requiring some averaging of the surrounding values [192]. It is also possible to increase the interpolation order by including more nodes within each element, leading to spectral element methods with exponential convergence properties as the order increases [194–197], although global surface smoothness is still not automatically ensured [195].

c. Subdivision methods Subdivision surface methods are becoming increasingly popular. They constitute a generalization of spline based approaches. Starting from a coarse unstructured control mesh of quadrilaterals or flat triangles, one successively introduces new nodes and

[2] Spring network models start from the basic assumption that the cytoskeleton of red blood cells can be appropriately modeled by not discretizing any continuum descriptions, but rather by mimicking the spectrin proteins *directly* with a, possibly coarser, triangulated mesh [158]. This idea originates from the observation that the expanded cytoskeleton forms a lattice-like network [190]. The actual membrane properties are implemented via appropriate potentials acting between the nodes, stemming from coarse-grained molecular or from reasonable ad-hoc models [158]. Connections of the associated potential strengths (spring constants) with continuum properties (elastic moduli) are then usually established by considering special cases of the mesh, such as regular hexagonal networks [189, 191].

elements according to certain predefined rules. A key observation is that any point on the limit surface obtained by an infinite number of refinements can be directly evaluated via some closed analytical formula. This enables easy and efficient computations of derivatives. Different variations of this idea exist. One needs to distinguish between interpolating (the original nodes are members of the limit surface) and approximating schemes (the original nodes are not necessarily located on the limit surface). The first ones have the advantage that the limit surface is more directly connected to the control mesh. However, the latter have the big advantage of being $\mathcal{C}^1$ smooth everywhere (even $\mathcal{C}^2$ at regular nodes[3]), whereas in the first case the curvatures are not always bounded [198]. This makes approximating approaches the dominant choice for dynamic simulations of soft objects. Two popular schemes are the Catmull-Clark (quadrilateral based) [199, 200] and especially the Loop (based on flat triangles) [55, 91, 96, 102, 198, 201–205] subdivision methods. We remark again that both reduce to $\mathcal{C}^1$ smoothness near irregular nodes. Hence, good mesh regularity is a requirement for accurate derivatives [27].

d. Spectral methods Another class are spectral methods where functions are expanded using some basis functions whose support extends over the whole domain (this is not to be confused with spectral element methods [194, 195], where the support of the individual high-order polynomials extend only over the elements). In the present biofluidic context, the surface itself and functions defined on it are usually expanded using spherical harmonics [84, 85, 92, 101, 103, 206–209]. They work best for nearly spherical shapes and can result in spectral accuracy (i.e. the error decays exponentially fast). Instead of spherical harmonics a simple Fourier series expansion is also possible, albeit rarely used [210].

e. Other methodologies An (almost) completely two times continuously differentiable surface may be constructed by using cubic B-Splines together with a structured mesh [211–213]. Unfortunately, for closed objects two singular poles occur where the derivatives are not well defined, requiring e.g. extrapolation of quantities [214] or the usage of a second (rotated [212] or unstructured [191]) mesh. Finally, NURBS [77] and fully three-dimensional phase field models have also been employed [215, 216].

B. Computation of bending forces

The surface discretizations described above can be combined with different methods to compute the actual bending forces, which we describe in this section. For the sake of completeness, we shortly mention in section III B 1 the computation of bending forces in the computationally much simpler case of two-dimensional and axisymmetric geometries. In full 3D, the wealth of available methods can be sorted into three categories: the *force formulation* (sec. III B 2) starts from the energy equation (2) and yields a force at each node. The *strong formulation* (sec. III B 3) and the *weak formulation* (sec. III B 4) on the other hand depart from the Euler-Lagrange equation (7) and yield a surface force density. Approaches based on the thin-shell formalism (including the linear bending models) are often implemented by means of the strong formulation. All methods have their advantages and disadvantages and there is currently no consensus on which one is the best for a specific application.

1. *Two-dimensional and axisymmetric models*

In two dimensions, the Helfrich bending energy (with zero reference curvature) is simply $E_\mathrm{B} = \frac{1}{2}\int H^2 \mathrm{d}s$, where s denotes a coordinate along the contour and the integration goes over the full perimeter of the particle. A variational derivative leads to [89, 90, 217]

$$\triangle \boldsymbol{f}_\mathrm{B} = \kappa_\mathrm{B}\left(\frac{\partial^2 H}{\partial s^2} + \frac{1}{2}H^3\right)\boldsymbol{n} \tag{10}$$

in analogy to equation (7). Different equivalent expressions are possible if the particle is locally inextensible [217]. The interface can be discretized by using for example straight lines [89, 90, 119, 218], level-set [219–223], phase field [88, 224, 225], spline [226] or Fourier methods [217, 227–229].

Axisymmetric algorithms start from the full 3D equations and reduce them by one dimension via the assumption of rotational symmetry. Differentiation and integration on the surfaces thus reduce to 1D problems. Approximations of the interfaces employ e.g. straight lines [230, 231], Fourier expansions [95, 232, 233], B-Splines [134], level-set [223] or phase field models [234–236].

2. *Direct application of the principle of virtual work (force formulation)*

In full 3D, the first possibility to numerically compute the forces from the bending energy E_B is to directly discretize the integral as well as the mean curvature appearing in equation (2). Thereafter, E_B depends explicitly on the node positions $\boldsymbol{x}^i$ with $i = 1, \ldots, N$, i.e. $E_\mathrm{B} = E_\mathrm{B}(\{\boldsymbol{x}^i\})$, where $\{\boldsymbol{x}^i\}$ means the collection of all N nodes. Contrary to the approaches presented in the following sections, this effectively makes the force formulation a discrete model. By the principle of virtual work, the force (in Newton) acted upon the membrane node $\boldsymbol{x}^i$ by the fluid is given by the gradient [109, 169, 237, 238]

$$\boldsymbol{F}(\boldsymbol{x}^i) = \frac{\partial E_\mathrm{B}(\{\boldsymbol{x}^i\})}{\partial \boldsymbol{x}^i}\,, \quad i = 1, \ldots, N\,. \tag{11}$$

[3] Regular nodes are defined by having 4 (quadrilaterals) or 6 (triangles) neighbor nodes.

Roughly speaking, this is a discretized version of the variational derivative leading to equation (7) [81, p. 93]. For many surface discretizations, the gradient can be computed analytically using the explicit expression for the discretized bending energy [27, 72]. Guckenberger *et al.* [27] named this method "force formulation" because it yields a force (rather than a force density) at each node.

Some flow solvers, e.g. boundary integral methods, require the force per unit area (traction jump) instead of the force. In this case, one divides by the area A_i associated with or "occupied" by the node:

$$\triangle \boldsymbol{f}_{\mathrm{B}}(\boldsymbol{x}^i) \approx \boldsymbol{F}(\boldsymbol{x}^i)/A_i\,, \quad i = 1, \ldots, N\,. \tag{12}$$

Using flat triangles, typical choices for A_i are 1/3 of the total area of the triangles surrounding $\boldsymbol{x}^i$ [86, 93, 98, 109] or Meyer's mixed area [27, 239]. The results presented in reference [27] suggest that the latter gives superior results since it leads to a perfect tiling of the surface (i.e. $\sum_{i=1}^{N} A_i = A$, where A is the total surface area).

We remark that although computationally convenient, the force formulation as a discrete model is observed to be more sensitive to the mesh regularity (i.e. to element area and connectivity variances) than the continuum approaches presented in sections III B 3 and III B 4 [81, p. 93] [27, ch. 3.5]. For sufficiently regular meshes, however, similar results can be achieved [27, ch. 3.5]. Also note that "pure" spring network models necessarily use the force formulation idea as they start with a discrete model in the first place.

Out of the various available surface discretizations described in section III A, the force formulation has thus far been used only with flat triangles and subdivision surface schemes.

a. Flat triangles Depending on the surface approximation, discretizing the integral and the mean curvature H in equation (2) within the force formulation can be done in different ways. Here we describe the two most often used possibilities for flat triangles (termed Method A and B in [27]).

Method A starts from an often used expression [28, 72, 105, 109, 117, 121–126, 147, 158, 169, 189, 240–251] similar to an angle-potential:

$$E_{\mathrm{B}} = 2\tilde{\kappa}_{\mathrm{B}} \sum_{\langle i,j \rangle} [1 - \cos(\theta_{ij} - \theta_{ij}^0)]\,. \tag{13}$$

Here, the sum runs over all edges $\langle i, j \rangle$ once, θ_{ij} is the angle between the normal vectors of the adjacent triangles with edge $\langle i, j \rangle$, θ_{ij}^0 indicates the reference (or spontaneous) angle and $\tilde{\kappa}_{\mathrm{B}}$ is an effective bending modulus. This formula can be connected to the Helfrich model from eq. (2) for special cases, such as a sphere approximated by equilateral triangles and zero reference curvature. In this case the effective and physical bending moduli are related by [241]

$$\tilde{\kappa}_{\mathrm{B}} = \sqrt{3}\,\kappa_{\mathrm{B}}\,. \tag{14}$$

Despite being rigorously valid only for this special mesh topology and geometry, the relation (14) is often also used in the general case.

Method B is based on a finite difference cotangent scheme for the Laplace-Beltrami operator (and thus also of the mean curvature H according to equation (4)). Note that different variants of this scheme can be found in the literature, obtainable e.g. by evaluating a contour integral [52, 98, 239]. Method B uses the discretization described in reference [241]:

$$\Delta_{\mathrm{S}} w(\boldsymbol{x}^i) \approx \frac{\sum_{j(i)} (\cot \vartheta_1^{ij} + \cot \vartheta_2^{ij})(w(\boldsymbol{x}^i) - w(\boldsymbol{x}^j))}{2A_{\mathrm{V}}^i}\,, \quad i = 1, \ldots, N\,. \tag{15}$$

w is some arbitrary function on the surface S, the sum goes over the next neighbors of node $\boldsymbol{x}^i$, A_{V}^i denotes its Voronoi area [239], and ϑ_1^{ij} and ϑ_2^{ij} are the angles opposite to the edge $\langle i, j \rangle$ in the triangles which contain nodes $\boldsymbol{x}^{j-1}$ and $\boldsymbol{x}^{j+1}$. See figure 1 for a sketch. This scheme is

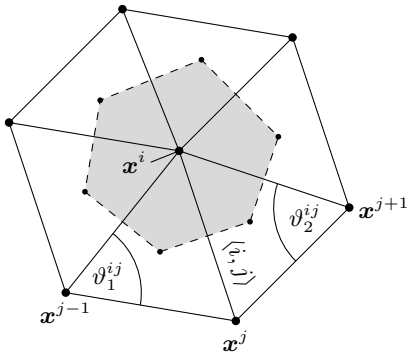

Figure 1. The first ring of neighbors around some node $\boldsymbol{x}^i$. The shaded region marks the Voronoi area A_{V}^i. Modified from [27] with permission from Elsevier.

used in reference [98] as well as references [106, 252] and subsequent publications [114, 115, 188, 253, 254].

Besides Methods A and B, many other possibilities exist such as including triangle areas as weights in eq. (13) [243] or using some other discretizations of the mean curvature [28, 237], also including the ones presented in the next section III B 3 a. The underlying problem of finding appropriate discretizations for the curvatures and the Laplace-Beltrami operator on triangulated meshes has attracted a lot of researchers from the mathematics and computer science communities since it is also of high relevance for other fields such as computer graphics or surface reconstruction. See for example the recent references [37, 239, 255–269]. Yet, one has to acknowledge that no perfect discretization of the Laplace-Beltrami operator can exist [260].

b. Subdivision schemes The "force formulation" is also compatible with other surface representations. For example, references [91, 96, 102] employed Loop's subdivision surface method and obtained the mean curvature

within elements by means of direct differentiation. Nodal values were computed by subsequent averaging.

3. *Computation by means of the Euler-Lagrange equation (strong formulation)*

Another possibility is to evaluate the Euler-Lagrange equation (7) or the equations from thin shell theory (cf. appendix A) directly. This requires as the most intricate ingredient an approximation for the Laplace-Beltrami operator of the mean curvature, $\Delta_S H$, i.e. a fourth order derivative. We note that Guckenberger *et al.* [27] termed this idea "variational formulation" because it uses the expression (7) which is obtained by variational calculus. Since, however, this term is also often used in connection with the finite element method (see sec. III B 4), we will denote it here as the "strong formulation". As in the previous section, the implementation details of the strong formulation depend on the underlying surface discretization.

a. Flat triangles One basic idea is to apply the same procedure that was used to compute the mean curvature H via eq. (4) again to $\Delta_S H$. For example, if H was computed with a cotangent scheme at all nodes, then $\Delta_S H$ can be approximated by applying the cotangent scheme to H itself. This is Method C in [27]. To be more precise, the authors employed eq. (15) except that the Voronoi area in the denominator was replaced with Meyer's mixed area [239] leading to a perfect tiling of the surface and thus to superior results when compared with Method B [27]. This approach (sometimes with slight changes) has often been used by other researchers (e.g. [37, 52, 66, 86, 93, 183, 255, 270–272]).

A second possibility for flat triangles is based on a kernel of the heat equation (Method D in [27]), and essentially consists of computing the sum of the distances between the evaluation point and *all* other vertices of the mesh weighted with an exponential decay [261]. Due to the global support, the convergence properties were found to be the best of all the considered methods, but at the price of a large performance impact [27]. This is most likely the reason why it has not been used in the biofluidic context before. We remark that a cutoff can be applied to increase performance, and that employing the geodesic distance (the distance along the surface) improves results further [269].

A third possibility uses parabolic fitting of the surface components and of the mean curvature around the evaluation point [107] (Method E in [27]). The robustness of this algorithm can be easily tuned by including more neighbors. Other fitting polynomials are also possible [273], with fourth or higher order polynomials allowing for a direct computation of $\Delta_S H$ in one go. Otherwise, several successive fits are necessary. Method E was used (sometimes in modified form) e.g. in references [37, 99, 107, 186, 272, 274–277]. References [94, 104, 146, 148, 278–285] use a combination of parabolic fitting for H and a direct discretization of the Laplace-Beltrami operator of H in the spirit of Method C. Moreover, as already mentioned in the force formulation section, countless other ways to discretize the Laplace-Beltrami operator on triangulated meshes exist (see sec. III B 2 a and the references provided therein).

So far we have only discussed approaches to compute the mean curvature H and its Laplace-Beltrami operator $\Delta_S H$. Yet, equation (7) also sports the Gaussian curvature K as well as the normal vector $\boldsymbol{n}$. Fortunately, since $\Delta_S H$ is often the dominating term (see appendix A 4 d) and they only contain second and first order derivatives, respectively, their approximations usually introduce only negligible errors [27]. If the parabolic fitting idea is used, both can be computed naturally from the fitted surface [107]. In case of the other two schemes (Methods C and D), it is convenient and quite accurate [27] to compute K by means of a discretized version of the Gauss-Bonnet theorem [239], and $\boldsymbol{n}$ via the "mean weighted by angle" algorithm [286].

b. Higher order elements Curved triangles allow the direct computation of the curvatures and normal vectors within the elements since all quantities are assumed to vary quadratically inside of them. Nevertheless, discontinuities arise at the nodes. As a solution, the resulting quantities are averaged. Afterwards, assuming that they vary quadratically, too, the final traction jump is computed for example by performing one derivative explicitly and the other by means of a contour integral [54, 83]. Spectral element methods have apparently not been used to compute equation (7).

c. Subdivision surfaces To the best of our knowledge, subdivision surface methods were not yet used to evaluate the local equilibrium condition (7) directly. This probably stems from the fact that they are mostly used together with the finite element method (sec. III B 4) in the general field of thin-shell analysis [198].

d. Spectral methods Here, the surface components [84, 101, 103, 207, 208] or sometimes only the radius [91, 92] are expanded into a spherical harmonics series. Evaluation of eq. (7) or of the thin shell theory equations from appendix A is then in principle straightforward since the derivatives act on the basis functions and are well-defined everywhere [287]. We provide more details in appendix B. However, because the mean curvature H decays only slowly in the spectral space, a comparably high number of modes must be used. This in turn often results in prohibitively slow performance in the evaluation of the hydrodynamics. The typical remedy is a procedure called de-aliasing: Generally speaking, one can use a relatively low resolution for the hydrodynamics, but upsample the grid (via spherical harmonics interpolation) for the purpose of computing the bending forces [84, 101, 103, 207]. A possible alternative might be to bypass the transformation of H and directly compute $\Delta_S H$ from the surface components, as remarked in the appendix.

Other spectral methods besides spherical harmonics were apparently not used so far for the purpose of 3D bending computations.

e. Other discretizations It is also possible to employ a level set [288] or combined level set method and essentially non-oscillatory (ENO) reconstruction [182] to directly evaluate equation (7). Using three-dimensional phase-field models is another possibility [215].

4. Finite element method (weak formulation)

In the third possibility to compute the bending forces, eq. (7) is multiplied with an arbitrary trial function (typically denoted $\delta\boldsymbol{x}$) and integrated over the membrane surface. Then the fourth order derivative of $\boldsymbol{x}$ is reduced to a second order derivative by means of two successive integrations by parts. These effectively move the derivatives to the trial functions $\delta\boldsymbol{x}$. Thus we find an integral equation constituting the so-called weak formulation of eq. (7) which can be solved by a finite element method (FEM) for $\triangle\boldsymbol{f}_\mathrm{B}$ [55, 149, 193, 198, 204, 289]. The basic idea here is to discretize the surface with some elements and expand the surface $\boldsymbol{x}$ as well as the trial functions $\delta\boldsymbol{x}$ in terms of a finite number of shape functions having local support on the elements. After substituting them into the integral equation, evoking the arbitrariness of $\delta\boldsymbol{x}$ and also discretizing the integral via some numerical quadrature, one ends up with a sparse linear system of equations that determines $\triangle\boldsymbol{f}_\mathrm{B}$ [55, 131].[4] Alternatively, the value of $\triangle\boldsymbol{f}_\mathrm{B}$ at some node can be *approximated* via the mean value theorem, dodging the explicit solution of the linear system [133, eq. (62)] [149].

Proper convergence requires that if the integrand contains an r'th derivative, then the elements must approximate the surface such that it is $\mathcal{C}^r$ within the elements and $\mathcal{C}^{r-1}$ at the element borders [289, ch. 3.6]. Hence, since the bending energy contains a second order derivative, the elements themselves should be $\mathcal{C}^2$, and $\mathcal{C}^1$ at their borders. This is similar to the force formulation (sec. III B 2) which also requires only a second order derivative, but is in stark contrast to the strong formulation (sec. III B 3) which requires that the surface is at least $\mathcal{C}^3$ (otherwise the fourth order derivative would not be well defined). Despite having similar requirements as the force formulation, so far it remains unclear whether the force or the weak formulation performs better with respect to *accuracy* if the same surface elements are employed. Overall, the major advantage of FEM seems to lie in its *stability* [193, 290], although rigorous comparisons with the other two alternatives are apparently missing.

Considering the differentiability requirements, subdivision surface methods are often used for this approach [55, 149, 198, 200], as for Method S in reference [27]. Splines [213, 291], NURBS [77] or mixed phase field models are also possible [216].

The $\mathcal{C}^1$ requirement can be bypassed by introducing the mean curvature H as an additional independent variable [26, 292]. Hence, the overall system to be solved for $\triangle\boldsymbol{f}_\mathrm{B}$ and H consists not only of the weak form of the Euler-Lagrange equation, but also of an additional equation (also in weak form) for the mean curvature. This system contains only first order derivatives and is thus amenable to discretizations with flat triangles, resulting in a stable scheme [26, eqs. (4.3) and (4.4)] [290, eq. (3.4f) or (4.15f)] [143, 292–294]. An alternative is to use curved triangles (which also form a $\mathcal{C}^0$ surface, as mentioned above) [295, 296].

As a side note, ref. [206] employs the weak formulation similar to FEM, but together with spherical harmonics (which have global support and thus the method cannot be really classified as FEM). By choosing a particular trial function $\delta\boldsymbol{x}$, they obtain an equation with the expansion coefficients for the traction jump on the one side, and an expression involving the known derivatives of $\delta\boldsymbol{x}$ on the other side. The traction jump in the spatial domain is then obtained by a simple backward transformation.

C. Comparison of a selection of methods

An easy way to analyze the performance of bending algorithms is to consider shapes for which analytical formulas for the traction jumps can be derived. Guckenberger *et al.* [27] studied methods originating from flat triangles (Methods A – E and S mentioned above) for the typical equilibrium shape of a red blood cell, see figure 2. Methods A and B use the force formulation, C – E the strong formulation, and Method S the finite element method. They computed the maximal and average errors of the numerically obtained traction jump with respect to the analytical result in all cases. The spontaneous curvature was set to zero.

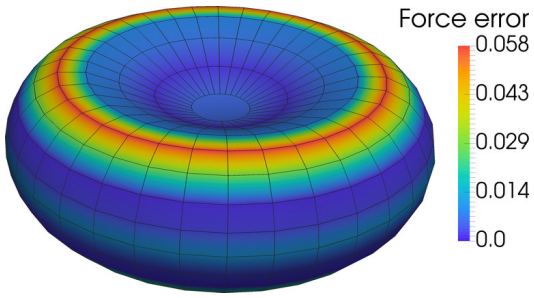

Figure 2. The typical shape of a red blood cell, as described by equation (B14). Intersections of the grid lines indicate the nodes used for the spherical harmonics expansion of order 16, and the color depicts the nodal errors of evaluating the traction jump (the maximum and average is shown in figure 4). Most other expansion orders show similar error patterns.

Their results for a certain type of mesh (called MT1 in

[4] In typical engineering applications the finite element method is applied the other way round, i.e. one usually solves for the expansion coefficients of the surface $\boldsymbol{x}$ while the traction is prescribed [193].

[27]) is shown in figure 3 for the mean curvature H, and in figure 4 for the traction jump $\triangle \boldsymbol{f}_\mathrm{B}$. Regarding the maximal error, none of the algorithms converge properly. Moreover, Method D, which appears to converge at least with a systematic error, also begins to diverge beyond a certain resolution when the mesh topology is slightly changed (mesh MT2 in [27], not repeated here).

For the average error, which is more relevant in Stokes flow applications, Method D appears to show proper convergence. Taking the MT2 mesh into account, all other algorithms roughly converge with a systematic error, except Method A which clearly diverges.

The authors of ref. [27] concluded that in principle the best scheme is Method D, although it is too slow for practical uses because it requires sufficiently high resolutions and scales as $\mathcal{O}(N^2)$ where N is the number of nodes. Hence, Method S or Method E are usually better choices. But note that the quality of the subdivision surface method S highly depends on the mesh regularity. See ref. [27] for more details and an in-depth discussion together with some guidelines.

Here we additionally include results obtained using the strong formulation with a spherical harmonics expansion of order p as described in appendix B. Figure 2 shows a typical error distribution for $\triangle \boldsymbol{f}_\mathrm{B}$ on the surface for $p = 16$. The errors for the mean curvature H drop to machine precision beyond an order $p \geqslant 5$, see figure 3. In this case the RBC surface is exactly representable by a spherical harmonics series of order 5. The mean curvature itself, on the other hand, cannot be expressed by just a few terms of the expansion owing to its highly nonlinear dependency on the surface geometry. As we compute the Laplace-Beltrami operator of H by expanding H again into spherical harmonics, the error decay of the traction jump in figure 4 occurs roughly exponentially (as is typical for spectral methods). If we computed the fourth order derivatives directly as remarked in the appendix, we would expect a jump to machine precision as for H. Hence we conclude that for spherical harmonics a somewhat more practical test would consider some non-exactly representable surface and assess its performance there. However, the main problem is to obtain precise reference results for such an object and we therefore leave this task for future work.

IV. APPLICATIONS

We will now summarize some important applications and provide an overview of the contexts in which the individual methods are being used.

A. Membranes in the absence of an externally imposed flow

The computation of equilibrium shapes of vesicles and red blood cells is a problem with a long history [17, 21, 34, 58, 68–70]. The goal is to find the minimum of the surface's energy under appropriate constraints. In case of vesicles this usually means to minimize the bending energy from eq. (2) or the extended version from eq. (9) (which includes the area-difference) under the constraints of constant surface area and volume. For red blood cells additional terms are needed to take the finite shear elasticities into account, although early works have neglected them.

To this end, it would in principle be possible to use the Euler-Lagrange equation (eq. (7) with $\triangle \boldsymbol{f}_\mathrm{B} = 0$ and appropriate amendments for the constraints) and solve it for the unknown shape directly. However, since it constitutes a 4th order nonlinear PDE, this is a formidable numerical task and was only attempted under the assumption of axisymmetry [58, 68–70, 142, 231, 297, 298]. Alternatively, the bending forces can be used to solve a damped equation of motion where the mass and the damping coefficients only influence the speed of convergence but do not modify the final equilibrium shapes. For example, Tsubota *et al.* [28, 147] used this approach together with flat triangles. A third and the most popular possibility is to perform a direct minimization of the energy via methods such as Monte Carlo [70, 139] or quadratic programming [141, 299]. This has been done for axisymmetric [223, 234] but also fully three-dimensional shapes. Employed discretizations include for example flat triangles (e.g. [70, 139, 243, 296, 299], and publications using Brakke's `Surface Evolver` [300] such as [301, 302]). Moreover, spherical harmonics [141, 303], subdivision surface methods [55] or B-Splines [213] have been used, sometimes in the framework of the finite element method [55, 213, 216].

In the related context of membrane thermal fluctuations, adequate simulations also require the inclusion of bending resistance. For example, [140, 304, 305] used spherical harmonics and [169] used a spring network model. Bending must also be included when considering the diffusion of nanoparticles near realistic red blood cells which was done in references [86, 306–309] via flat triangles and Method C from section III B 3.

In table I we list an overview of all works simulating isolated soft objects with or without an external flow together with the employed bending algorithms.

B. A single object in flow

The behavior of even a single soft object such as a vesicle, capsule or red blood cell in simple flows can be amazingly complex [1–5, 97], even bearing the possibility for deterministic chaos [310, 311]. For vesicles the dynamics is mostly determined by bending forces in connection with area inextensibility and volume conservation. Red blood cells are mostly dominated by shear elasticity, although the maximal deformation can be notably reduced by the bending resistance [54] and it prevents the formation of sharp cusps [312]. For very thin-shelled

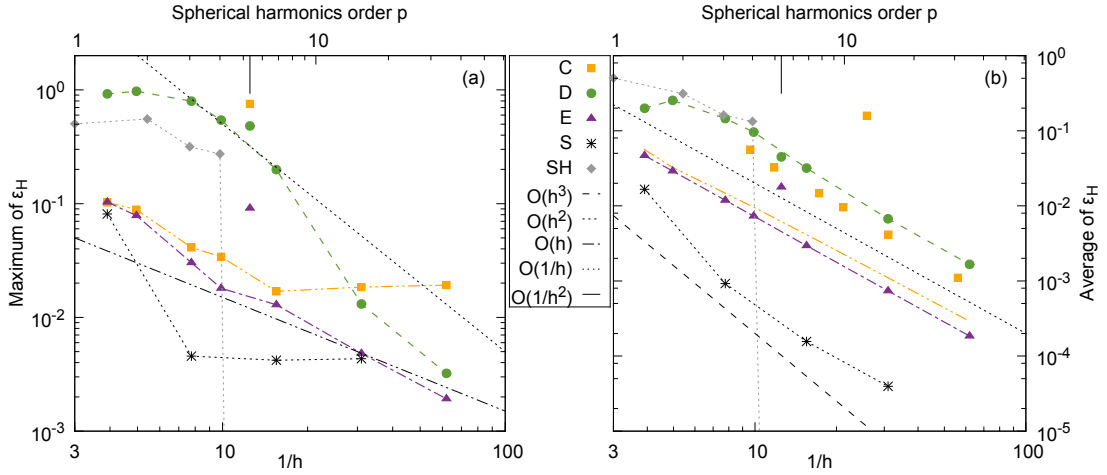

Figure 3. (a) Maximal and (b) average errors of the mean curvature H for the discocyte shape from figure 2. Methods C – E and S use flat triangles with a mean edge length of h (inverse on the lower x-axis). The lines are meant as guides to the eye to assess the typical convergence behavior. The vertical line at the top indicates results for an inhomogeneous triangulated mesh. Data for Methods A – E and S from reference [27] (MT1 mesh). The result for the spherical harmonics method SH is shown as a function of the truncation order p (upper x-axis, *no correlation* with the lower axis exists). Note that the error drops to machine precision ($\approx 10^{-14}$ for double precision arithmetic) for $p \geqslant 5$. Errors for the Gaussian curvature K are very similar.

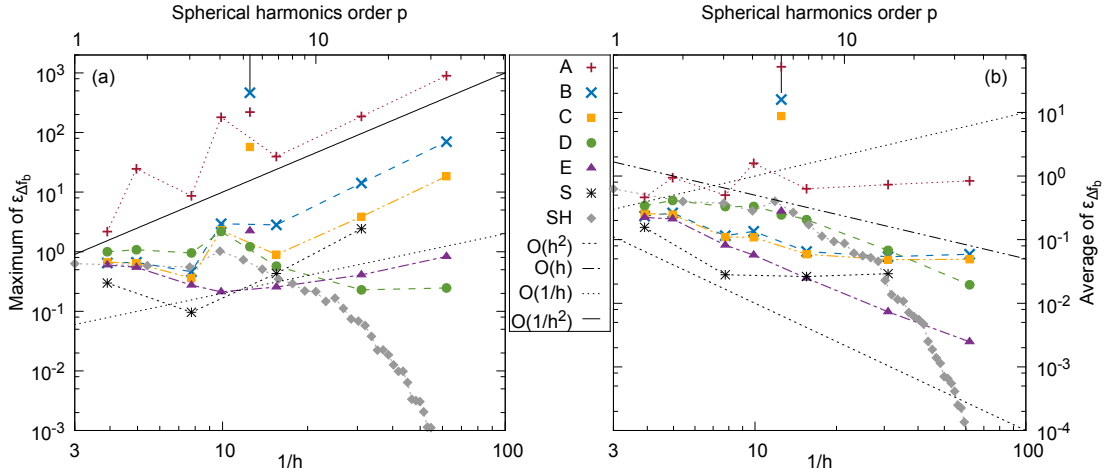

Figure 4. (a) Maximal and (b) average errors of the traction jump $\triangle \boldsymbol{f}_B$ for the discocyte shape from figure 2. Setup and symbols similar to figure 3. Data for Methods A – E and S from reference [27] (MT1 mesh). Errors for $\Delta_S H$ look very similar.

capsules, bending forces are often assumed to be negligible [5]. They only manifest in zones of negative stress where they define the wavelength of the emerging wrinkles [5, 72, 211, 212, 313, 314]. Recent works in this category are also collected in table I.

Two prototypical flows are commonly used: linear shear flows and Poiseuille flows. The former is somewhat simpler as the incoming flow far away from the object possesses a spatially constant shear rate while the latter is somewhat more relevant for applications in micro- or biofluidics. Occasionally, also time-dependent flows have been investigated [280, 315–319].

1. *Linear shear flows*

a. Spherical capsules The influence of bending resistance has been systematically studied almost only for an initially spherical elastic capsule endowed with additional bending rigidity in linear shear flows. The capsule at low shear rates deforms into an approximate ellipsoid and performs a tank-treading motion, i.e. the membrane rotates around the stationary shape. This is illustrated in figure 5 (a). The system parameters can be cast into three dimensionless values: the dimensionless shear rate (or elastic capillary number) $G = \mu\gamma R/\kappa_S$, the dimensionless ratio between shear and bending resistance $\hat{\kappa}_B = \kappa_B/(R^2\kappa_S)$ and the viscosity ratio $\lambda = \mu_C/\mu$. Here, κ_S is the shear

Discretization	Force formulation	strong formulation (Euler-Lagrange)	weak formulation (FEM)
Flat triangles	A [18, 27, 28, 105, 123, 147, 169, 180, 189, 243, 244, 247–249] B [27, 98, 106, 115, 188, 252, 253]	C [27, 52, 66, 86, 93, 183, 270, 271, 279, 306–309, 320, 321] D [27] E [27, 99, 107, 275–277] C + E [94, 104, 146, 148, 278–282]	[143, 293]
Higher order elements (curved triangles)		[54, 83]	[296]
Subdivision methods	[91, 102]		[27, 55, 149, 200, 204, 205]
Spectral methods (spherical harmonics)		[84, 85, 91, 92, 207, 209, 322, 323]	[206]*
Other methods		[182, 215]	

Table I. Overview of recent numerical works for a single object with or without external flow that compute the bending forces using full 3D methodologies. We only list publications that use the Helfrich bending law or a linear bending model (see section II A 2 b). Methods A – E have been shortly described in sec. III B and in detail in reference [27]. Note that the discretizations only refer to the computation of the bending forces (other components of the solvers might use different approaches). *Reference [206] uses the weak formulation but not the FEM, as explained in section III B 4.

modulus for the in-plane tensions (usually modeled by the neo-Hookean law [5, 27]), R the initial radius, μ the dynamic viscosity of the ambient fluid, μ_C the dynamic viscosity of the internal fluid, and γ the shear rate. Note that different conventions for the moduli exist in the literature. The reference state for the in-plane tensions is taken to be the initial sphere and the bending reference state is usually a flat sheet ($H_0 = 0$).

The shape is typically described by the Taylor deformation parameter $D = \frac{a-c}{a+c}$ with the largest and smallest semi axes a and c, respectively, and the inclination angle θ between the x-axis and a. D and θ can be extracted from an ellipsoid with the same inertia tensor [192, 238]. Without bending forces, ample data is available because this setup is very often used for the verification of hydrodynamic simulation codes. There is very good agreement across a wide range of surface discretizations and flow solvers as shown in figure 5 (b).

Once bending forces are included, however, one observes a surprisingly large spread of the values reported in the literature as shown in figure 5 (c). Since all simulations are intended to model the same physical situation, this spread is somewhat unexpected. Given the excellent agreement without bending forces in figure 5 (b), a decisive influence of the flow solver is unlikely. The fact that some of the references use a linear bending model is also most likely not the reason as the curves in question do not match among themselves and because the $\Delta_S H$ term (which is common to all) should dominate the behavior (compare sec. A 5). Moreover, not even results using the same surface discretization methodologies agree with each other. This spread thus clearly exemplifies the difficulty of accurately computing the bending forces. In the future, it would be interesting to conduct similar studies including a non-zero spontaneous curvature.

b. Non-spherical objects Vesicles typically obey strict area and volume conservation and thus, for any deformation to be possible, the initial shape must not be a sphere. This adds an additional dimensionless parameter called the reduced volume $\nu = 6\sqrt{\pi}V/S^{3/2} \leqslant 1$ [325], where $\nu = 1$ corresponds to a sphere. Owing to the excess area, additional phenomena such as vacillating-breathing, tumbling or kayaking motions arise (see references [9, 92, 93, 102, 143, 253, 271, 325] and the reviews [4, 97]). Similar features are shown by capsules [206, 326, 327]. The dynamics of red blood cells ($\nu \approx 0.6$ [1, 271]) can be even richer, adding states like breathing or tilted tank-treading [3, 10, 32, 66, 146, 181, 248, 278, 281, 328–331]. Finally, spatial variations of the bending modulus can lead to self-propelled [67] or migrating [332] particles.

2. *Poiseuille flows*

Studies of vesicles in bounded or unbounded Poiseuille flows are scarcer than for linear shear flows. Known shapes for vesicles include bullets, parachutes, croissants and static slippers [275, 333–335]. Red blood cells add states known from linear shear flows (e.g. tumbling), but also novel ones such as snaking or “dynamic” slippers

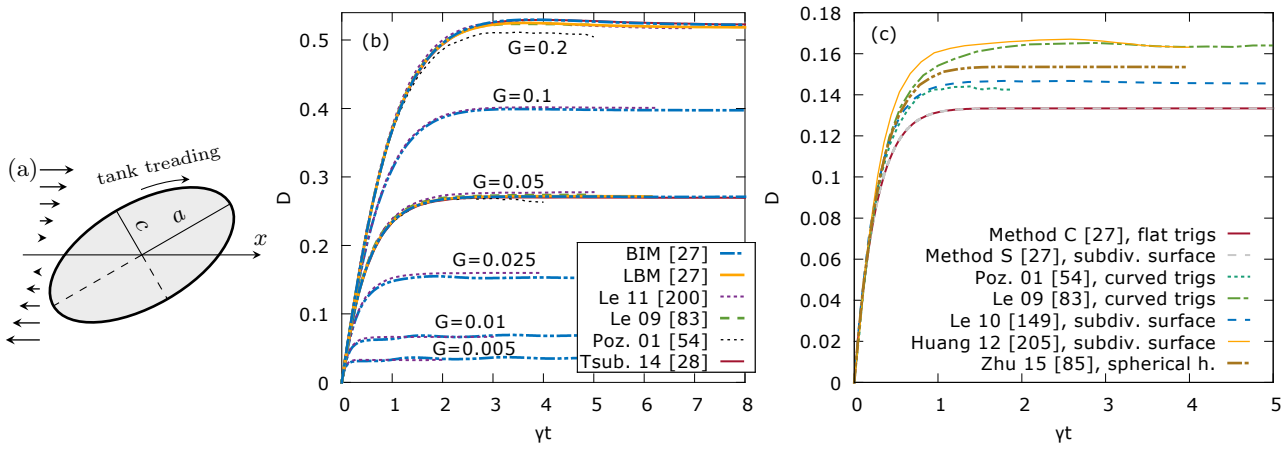

Figure 5. Results from 3D simulations of an initially spherical capsule under the influence of a linear shear flow. (a) 2D sketch. a is the largest and c the smallest half axis. "Tank treading" refers to the rotation of the membrane around the object's centroid while the shape remains constant. (b) Time evolution of the Taylor deformation parameter D for various dimensionless shear rates G *without* bending resistance as a function of the dimensionless time γt. Viscosity ratio $\lambda = 1$. Results by Huang et al. [205], Le [149] and Zhu and Brandt [85] are not included for clarity but match well with BIM. (c) Comparison of the recent literature for $G = 0.05$ and $\hat{\kappa}_B = 0.0375$, i.e. with some bending resistance included. Viscosity ratio $\lambda = 1$. Method C was introduced in section III B 3 a, Method S in section III B 4. All references use the same physical models and parameters, except for Pozrikidis [54] who used a Hookean elastic law. All use the Helfrich or a linear bending model (cf. sec. II A 2 b), except Huang et al. [205] who employ the bending model introduced by Zarda et al. [324]. However, the employed flow and discretization algorithms vary greatly. (a), (b) and (c) modified from [27] with permission from Elsevier.

[18, 97, 153, 188, 248, 336]. Moreover, the transition from the discocyte to the parachute shape was shown to depend on the bending modulus for vesicles as well as cells [188, 248].

C. Several particles under flow

In many real-world situations, soft objects are not isolated but occur in suspensions. Numerical studies on very diluted [13, 18, 114, 115, 337–339] and medium to dense [72, 109, 110, 117, 121–123, 125, 126, 250, 251, 283–285, 340–350] RBC suspensions are relatively abundant. Also see references [8, 18, 20, 32, 33, 351] for recent reviews. On the other hand, 3D simulations of interacting vesicles or capsules are quite rare. For example, two or more capsules have been simulated without [214, 352–357] and sometimes with [129, 358, 359] some bending rigidity in 3D. Numerical studies of interacting vesicles were mostly limited to 2D so far (e.g. [13, 217, 337, 360–365]), with the notable exception of reference [96]. Also note that references [101, 103, 208, 293] touched the subject but focused on the development of the numerical method rather than on physical results.

In table II we give an overview of recent works in conjunction with the employed bending algorithm. Interestingly, most simulations are based on flat triangles and very often use Method A from equation (13). The most likely reason for this is the algorithm's simplicity and efficiency in terms of the number of arithmetic operations, although ref. [27] found that it requires comparably small time steps. Its lack of high fidelity seems to be of only minor concern for red blood cell suspension simulations given the relative smallness of and uncertainty in experimentally determined bending moduli (and spontaneous curvature), the variation of RBC properties with age [153, 163, 370–372], and the routinely neglected influence of the vessel wall's glycocalyx [373, 374]. Hence, effects that are also observed *in vivo* must have a certain robustness and low-accuracy bending methods may be acceptable for these applications, although systematic studies have not been conducted so far.

V. SUMMARY AND FUTURE PERSPECTIVES

Bending forces are an integral component of many simulation codes for the study of natural or artificial soft particle suspensions. While the complexity of solving the Navier-Stokes equations for the hydrodynamic flow has long been recognized, the computational difficulties of computing bending forces have not always been fully appreciated.

In this review, we attempted to give an overview of the various approaches for bending forces developed during the last decades. We focused on membranes whose bending energy can be described by the famous Helfrich model. The described methods can be classified into three broad categories which are termed the *force*, the *strong* (or Euler-Lagrange) and the *weak* formulation. In addition, bending algorithms can be combined with different ways to discretize the surface itself. *Flat triangles*, *spherical*

Discretization	Force formulation	strong formulation (Euler-Lagrange)	weak formulation (FEM)
Flat triangles	A [18, 72, 109, 117, 118, 121–126, 245, 246, 250, 251, 340, 342, 344–350, 359, 366, 367] B [114, 115, 254]	C [110] E (only H) [186, 274] C + E [283–285]	[293]
Subdivision methods	[96]		[358]
Spectral methods (spherical harmonics)		[84, 101, 103, 207, 208, 341, 343, 368, 369]	

Table II. Overview of recent numerical works using full 3D methodologies similar to table I, but for the interaction of several particles ($\geqslant 2$) in external flows.

harmonics and *subdivision* schemes are the most widely used methods. Almost all of the described bending algorithms are currently being used in modern simulations of soft objects in flows. Yet, the simple case of a capsule in a linear shear flow clearly shows that the numerically predicted dynamics are in fairly good agreement with each other only if bending effects are neglected. As soon as bending forces are included, the various implementations start to scatter rather widely.

For future research, both numerical and physical issues come to mind. Numerically, an important task would be a systematic study on how the different bending algorithms behave when combined with different surface discretizations. While such a comparison has been attempted for flat triangles and spherical harmonics in section III C, it does not yet provide a clear and systematic distinction between the force, strong and weak formulations. It would certainly be worthwhile to study the advantages and disadvantages of the three methodologies more systematically, which would require to use the same surface discretization in all three cases. The ultimate goal would be to establish a definite reference algorithm that is proven to provide correct and especially robust results and at the same time has practical performance for dynamic simulations with many particles. Furthermore, it is at present also unclear if and how the quality of the various algorithms would change once a spontaneous curvature is included.

On the more physical side it would be interesting to systematically assess the influence of the bending rigidity and/or spontaneous curvature for the practically relevant case of a soft object in Poiseuille flow similar to what has been done in shear flow. Moreover, the effect of the bending resistance on the behavior of dense suspensions (speed of margination, formation and thickness of the cell-free layer, etc.) appears to not have been systematically considered so far.

The final issue concerns the spontaneous curvature H_0. Although a noticeable influence of H_0 on the behavior of a single cell in flow has been found in a recent simulation study [66], a consensus on whether a spontaneous curvature should be included e.g. for red blood cells, and, if so, what its value should be, seems currently not in sight. Presumably, only novel sophisticated experiments can help to fully settle this question.

ACKNOWLEDGMENTS

The authors would like to thank A. Daddi-Moussa-Ider for helpful discussions. Funding from the Volkswagen Foundation and computing time granted by the Leibniz-Rechenzentrum on SuperMUC are gratefully acknowledged by A. Guckenberger and S. Gekle. A. Guckenberger additionally thanks the Elitenetzwerk Bayern (ENB), Macromolecular Science, for their support.

[1] C. Misbah, *"Vesicles, capsules and red blood cells under flow,"* J. Phys.: Conf. Ser. **392**, 012005 (2012).

[2] P. M. Vlahovska, D. Barthes-Biesel, and C. Misbah, *"Flow dynamics of red blood cells and their biomimetic counterparts,"* Comptes Rendus Phys. **14**, 451 (2013).

[3] A. Viallat and M. Abkarian, *"Red blood cell: From its mechanics to its motion in shear flow,"* Int. Jnl. Lab. Hem. **36**, 237 (2014).

[4] D. Abreu, M. Levant, V. Steinberg, and U. Seifert, *"Fluid vesicles in flow,"* Adv. Colloid Interface Sci. **208**, 129 (2014).

[5] D. Barthès-Biesel, *"Motion and Deformation of Elastic Capsules and Vesicles in Flow,"* Annu. Rev. Fluid Mech. **48**, 25 (2016).

[6] N. Mohandas and P. G. Gallagher, *"Red cell membrane: Past, present, and future,"* Blood **112**, 3939 (2008).

[7] Y. Kim, K. Kim, and Y. Park, in *Blood Cell - An Overview of Studies in Hematology*, edited by T. Moschandreou (InTech, 2012) pp. 167–194.

[8] J. B. Freund, *"Numerical Simulation of Flowing Blood Cells,"* Annu. Rev. Fluid Mech. **46**, 67 (2014).

[9] M. Guedda, M. Abaidi, M. Benlahsen, and C. Misbah, *"Dynamic modes of quasispherical vesicles: Exact analytical solutions,"* Phys. Rev. E **86**, 051915 (2012).

[10] J. Dupire, M. Socol, and A. Viallat, *"Full dynamics of a red blood cell in shear flow,"* Proc. Natl. Acad. Sci. **109**, 20808 (2012).

[11] C. Minetti, T. Podgorski, G. Coupier, and F. Dubois, *"Fully automated digital holographic processing for monitoring the dynamics of a vesicle suspension under shear flow,"* Biomed. Opt. Express **5**, 1554 (2014).

[12] Y.-S. Choi and S.-J. Lee, *"Three-dimensional volumetric measurement of red blood cell motion using digital holographic microscopy,"* Appl. Opt. **48**, 2983 (2009).

[13] V. Clavería, O. Aouane, M. Thiébaud, M. Abkarian, G. Coupier, C. Misbah, T. John, and C. Wagner, *"Clusters of red blood cells in microcapillary flow: Hydrodynamic versus macromolecule induced interaction,"* Soft Matter **12**, 8235 (2016).

[14] F. Merola, P. Memmolo, L. Miccio, R. Savoia, M. Mugnano, A. Fontana, G. D'Ippolito, A. Sardo, A. Iolascon, A. Gambale, and P. Ferraro, *"Tomographic Flow Cytometry by Digital Holography,"* Light Sci. Appl. **6**, e16241 (2017).

[15] V. Cristini and G. S. Kassab, *"Computer Modeling of Red Blood Cell Rheology in the Microcirculation: A Brief Overview,"* Ann. Biomed. Eng. **33**, 1724 (2005).

[16] C. Pozrikidis, ed., *Computational Hydrodynamics of Capsules and Biological Cells*, Chapman & Hall/CRC Mathematical and Computational Biology Series (CRC Press, Boca Raton, 2010).

[17] X. Li, P. M. Vlahovska, and G. E. Karniadakis, *"Continuum- and particle-based modeling of shapes and dynamics of red blood cells in health and disease,"* Soft Matter **9**, 28 (2013).

[18] D. A. Fedosov, H. Noguchi, and G. Gompper, *"Multiscale modeling of blood flow: From single cells to blood rheology,"* Biomech Model Mechanobiol **13**, 239 (2014).

[19] M. Ju, S. S. Ye, B. Namgung, S. Cho, H. T. Low, H. L. Leo, and S. Kim, *"A review of numerical methods for red blood cell flow simulation,"* Comput. Methods Biomech. Biomed. Engin. **18**, 130 (2015).

[20] G. Gompper and D. A. Fedosov, *"Modeling microcirculatory blood flow: Current state and future perspectives,"* WIREs Syst Biol Med **8**, 157 (2016).

[21] P. B. Canham, *"The minimum energy of bending as a possible explanation of the biconcave shape of the human red blood cell,"* J. Theor. Biol. **26**, 61 (1970).

[22] W. Helfrich, *"Elastic Properties of Lipid Bilayers: Theory and Possible Experiments,"* Z. Naturforsch. C **28**, 693 (1973).

[23] E. A. Evans, *"Bending Resistance and Chemically Induced Moments in Membrane Bilayers,"* Biophys. J. **14**, 923 (1974).

[24] J. L. Weiner, *"On a Problem of Chen, Willmore, et al,"* Indiana Univ. Math. J. **27**, 19 (1978).

[25] K. Deckelnick, G. Dziuk, and C. M. Elliott, *"Computation of geometric partial differential equations and mean curvature flow,"* Acta Numer. **14**, 139 (2005).

[26] G. Dziuk, *"Computational parametric Willmore flow,"* Numer. Math. **111**, 55 (2008).

[27] A. Guckenberger, M. P. Schraml, P. G. Chen, M. Leonetti, and S. Gekle, *"On the bending algorithms for soft objects in flows,"* Comput. Phys. Comm. **207**, 1 (2016).

[28] K.-i. Tsubota, *"Short note on the bending models for a membrane in capsule mechanics: Comparison between continuum and discrete models,"* J. Comput. Phys. **277**, 320 (2014).

[29] A. Prosperetti and G. Tryggvason, eds., *Computational Methods for Multiphase Flow* (Cambridge University Press, Cambridge, 2007).

[30] F. L. Brown, *"Elastic Modeling of Biomembranes and Lipid Bilayers,"* Annu. Rev. Phys. Chem. **59**, 685 (2008).

[31] A. S. Popel and P. C. Johnson, *"Microcirculation and Hemorheology,"* Annu. Rev. Fluid Mech. **37**, 43 (2005).

[32] T. Omori, Y. Imai, K. Kikuchi, T. Ishikawa, and T. Yamaguchi, *"Hemodynamics in the Microcirculation and in Microfluidics,"* Ann Biomed Eng **43**, 238 (2014).

[33] A. L. Fogelson and K. B. Neeves, *"Fluid Mechanics of Blood Clot Formation,"* Annu. Rev. Fluid Mech. **47**, 377 (2015).

[34] U. Seifert, *"Configurations of fluid membranes and vesicles,"* Adv. Phys. **46**, 13 (1997).

[35] C. Pozrikidis, *"Interfacial Dynamics for Stokes Flow,"* J. Comput. Phys. **169**, 250 (2001).

[36] M. Deserno, *"Fluid lipid membranes: From differential geometry to curvature stresses,"* Chem. Phys. Lipids **185**, 11 (2015).

[37] G. Xu, *"Discrete Laplace–Beltrami operators and their convergence,"* Comput. Aided Geom. Des. **21**, 767 (2004).

[38] R. Capovilla, J. Guven, and J. A. Santiago, *"Lipid membranes with an edge,"* Phys. Rev. E **66**, 021607 (2002).

[39] R. Capovilla, J. Guven, and J. A. Santiago, *"Deformations of the geometry of lipid vesicles,"* J. Phys. A: Math. Gen. **36**, 6281 (2003).

[40] Z. C. Tu and Z. C. Ou-Yang, *"Lipid membranes with free edges,"* Phys. Rev. E **68**, 061915 (2003).

[41] D. Steigmann, E. Baesu, R. Rudd, J. Belak, and M. McElfresh, *"On the variational theory of cell-membrane equilibria,"* Interfaces Free Boundaries **5**, 357

(2003).
[42] Z. Yao, R. Sknepnek, C. K. Thomas, and M. O. de la Cruz, *"Shapes of pored membranes,"* Soft Matter **8**, 11613 (2012).
[43] E. Baesu, R. E. Rudd, J. Belak, and M. McElfresh, *"Continuum modeling of cell membranes,"* Int. J. Non-Linear Mech. **39**, 369 (2004).
[44] A. Fogden, S. T. Hyde, and G. Lundberg, *"Bending energy of surfactant films,"* J. Chem. Soc., Faraday Trans. **87**, 949 (1991).
[45] V. A. Harmandaris and M. Deserno, *"A novel method for measuring the bending rigidity of model lipid membranes by simulating tethers,"* J. Chem. Phys. **125**, 204905 (2006).
[46] H. Møllmann, *Introduction to the Theory of Thin Shells* (John Wiley and Sons, New York, 1981).
[47] E. Ventsel and T. Krauthammer, *Thin Plates and Shells: Theory, Analysis, and Applications* (CRC Press, New York, 2001).
[48] S. Knoche and J. Kierfeld, *"Buckling of spherical capsules,"* Phys. Rev. E **84**, 046608 (2011).
[49] B. Seguin and E. Fried, *"Microphysical derivation of the Canham–Helfrich free-energy density,"* J. Math. Biol. **68**, 647 (2013).
[50] B. Kheyfets, T. Galimzyanov, A. Drozdova, and S. Mukhin, *"Analytical calculation of the lipid bilayer bending modulus,"* Phys. Rev. E **94**, 042415 (2016).
[51] F. Campelo, C. Arnarez, S. J. Marrink, and M. M. Kozlov, *"Helfrich model of membrane bending: From Gibbs theory of liquid interfaces to membranes as thick anisotropic elastic layers,"* Adv. Colloid Interface Sci. **208**, 25 (2014).
[52] G. Boedec, M. Leonetti, and M. Jaeger, *"3D vesicle dynamics simulations with a linearly triangulated surface,"* J. Comput. Phys. **230**, 1020 (2011).
[53] L. D. Landau and E. M. Lifshitz, *Theory of Elasticity*, 3rd ed., Course of Theoretical Physics No. 7 (Pergamon Press, Oxford, 1986).
[54] C. Pozrikidis, *"Effect of membrane bending stiffness on the deformation of capsules in simple shear flow,"* J. Fluid Mech. **440**, 269 (2001).
[55] F. Feng and W. S. Klug, *"Finite element modeling of lipid bilayer membranes,"* J. Comput. Phys. **220**, 394 (2006).
[56] H. J. Lee, E. L. Peterson, R. Phillips, W. S. Klug, and P. A. Wiggins, *"Membrane shape as a reporter for applied forces,"* Proc. Natl. Acad. Sci. **105**, 19253 (2008).
[57] T. R. Powers, *"Dynamics of filaments and membranes in a viscous fluid,"* Rev. Mod. Phys. **82**, 1607 (2010).
[58] J. T. Jenkins, *"Static equilibrium configurations of a model red blood cell,"* J. Math. Biology **4**, 149 (1977).
[59] O.-Y. Zhong-can and W. Helfrich, *"Instability and Deformation of a Spherical Vesicle by Pressure,"* Phys. Rev. Lett. **59**, 2486 (1987).
[60] O.-Y. Zhong-Can and W. Helfrich, *"Bending energy of vesicle membranes: General expressions for the first, second, and third variation of the shape energy and applications to spheres and cylinders,"* Phys. Rev. A **39**, 5280 (1989).
[61] R. Capovilla and J. Guven, *"Stresses in lipid membranes,"* J. Phys. A: Math. Gen. **35**, 6233 (2002).
[62] J. Guven, *"Membrane geometry with auxiliary variables and quadratic constraints,"* J. Phys. A: Math. Gen. **37**, L313 (2004).
[63] M. A. Lomholt and L. Miao, *"Descriptions of membrane mechanics from microscopic and effective two-dimensional perspectives,"* J. Phys. A: Math. Gen. **39**, 10323 (2006).
[64] A. Laadhari, C. Misbah, and P. Saramito, *"On the equilibrium equation for a generalized biological membrane energy by using a shape optimization approach,"* Phys. Nonlinear Phenom. **239**, 1567 (2010).
[65] G. Napoli and L. Vergori, *"Equilibrium of nematic vesicles,"* J. Phys. Math. Theor. **43**, 445207 (2010).
[66] K. Sinha and M. D. Graham, *"Dynamics of a single red blood cell in simple shear flow,"* Phys. Rev. E **92**, 042710 (2015).
[67] P. Olla, *"Tank-treading as a means of propulsion in viscous shear flows,"* J. Fluid Mech. **680**, 265 (2011).
[68] W. Helfrich and H. J. Deuling, *"Some theoretical shapes of red blood cells,"* J. Phys. Colloques **36**, C1 (1975).
[69] U. Seifert, K. Berndl, and R. Lipowsky, *"Shape transformations of vesicles: Phase diagram for spontaneous-curvature and bilayer-coupling models,"* Phys. Rev. A **44**, 1182 (1991).
[70] G. H. W. Lim, M. Wortis, and R. Mukhopadhyay, in *Soft Matter, Vol. 4: Lipid Bilayers and Red Blood Cells*, Soft Matter No. 4, edited by G. Gompper and M. Schick (Wiley-VCH, Weinheim, 2008) pp. 83–249.
[71] C. Pozrikidis, *Boundary Integral and Singularity Methods for Linearized Viscous Flow*, Cambridge Texts in Applied Mathematics No. 8 (Cambridge University Press, New York, 1992).
[72] T. Krüger, *Computer Simulation Study of Collective Phenomena in Dense Suspensions of Red Blood Cells under Shear* (Vieweg+Teubner Verlag, Wiesbaden, 2012).
[73] J.-B. Fournier, *"On the stress and torque tensors in fluid membranes,"* Soft Matter **3**, 883 (2007).
[74] M. Arroyo and A. DeSimone, *"Relaxation dynamics of fluid membranes,"* Phys. Rev. E **79**, 031915 (2009).
[75] J. T. Jenkins, *"The Equations of Mechanical Equilibrium of a Model Membrane,"* SIAM J. Appl. Math. **32**, 755 (1977).
[76] D. J. Steigmann, *"Fluid Films with Curvature Elasticity,"* Arch. Ration. Mech. Anal. **150**, 127 (1999).
[77] R. A. Sauer, T. X. Duong, K. K. Mandadapu, and D. J. Steigmann, *"A stabilized finite element formulation for liquid shells and its application to lipid bilayers,"* J. Comput. Phys. **330**, 436 (2017).
[78] P. M. Naghdi, in *Linear Theories of Elasticity and Thermoelasticity: Linear and Nonlinear Theories of Rods, Plates, and Shells*, Mechanics of Solids No. 2, edited by C. Truesdell (Springer Berlin Heidelberg, 1973) pp. 425–640.
[79] T. W. Secomb, *"Interaction between bending and tension forces in bilayer membranes,"* Biophys. J. **54**, 743 (1988).
[80] C. Pozrikidis, *"Numerical Simulation of the Flow-Induced Deformation of Red Blood Cells,"* Ann. Biomed. Eng. **31**, 1194 (2003).
[81] C. Pozrikidis, ed., *Modeling and Simulation of Capsules and Biological Cells*, Chapman & Hall/CRC Mathematical Biology and Medicine Series (Chapman & Hall/CRC, Boca Raton, FL, 2003).
[82] C. Pozrikidis, *"Resting shape and spontaneous membrane curvature of red blood cells,"* Math. Med. Biol. **22**, 34 (2005).
[83] D. V. Le, J. White, J. Peraire, K. M. Lim, and B. C. Khoo, *"An implicit immersed boundary method for three-*

dimensional fluid–membrane interactions," J. Comput. Phys. **228**, 8427 (2009).

[84] H. Zhao, A. H. Isfahani, L. N. Olson, and J. B. Freund, *"A spectral boundary integral method for flowing blood cells,"* J. Comput. Phys. **229**, 3726 (2010).

[85] L. Zhu and L. Brandt, *"The motion of a deforming capsule through a corner,"* J. Fluid Mech. **770**, 374 (2015).

[86] A. Daddi-Moussa-Ider, A. Guckenberger, and S. Gekle, *"Long-lived anomalous thermal diffusion induced by elastic cell membranes on nearby particles,"* Phys. Rev. E **93**, 012612 (2016).

[87] R. Skalak, N. Ozkaya, and T. C. Skalak, *"Biofluid Mechanics,"* Annu. Rev. Fluid Mech. **21**, 167 (1989).

[88] S. Aland, S. Egerer, J. Lowengrub, and A. Voigt, *"Diffuse interface models of locally inextensible vesicles in a viscous fluid,"* J. Comput. Phys. **277**, 32 (2014).

[89] I. Cantat and C. Misbah, in *Transport and Structure*, Lecture Notes in Physics No. 532-532, edited by S. C. Müller, J. Parisi, and W. Zimmermann (Springer Berlin Heidelberg, 1999) pp. 93–136.

[90] B. Kaoui, G. Ristow, I. Cantat, C. Misbah, and W. Zimmermann, *"Lateral migration of a two-dimensional vesicle in unbounded Poiseuille flow,"* Phys. Rev. E **77**, 021903 (2008).

[91] H. Zhao, A. P. Spann, and E. S. G. Shaqfeh, *"The dynamics of a vesicle in a wall-bound shear flow,"* Phys. Fluids **23**, 121901 (2011).

[92] H. Zhao and E. S. G. Shaqfeh, *"The dynamics of a vesicle in simple shear flow,"* J. Fluid Mech. **674**, 578 (2011).

[93] T. Biben, A. Farutin, and C. Misbah, *"Three-dimensional vesicles under shear flow: Numerical study of dynamics and phase diagram,"* Phys. Rev. E **83**, 031921 (2011).

[94] A. Yazdani and P. Bagchi, *"Three-dimensional numerical simulation of vesicle dynamics using a front-tracking method,"* Phys. Rev. E **85**, 056308 (2012).

[95] H. Zhao and E. S. G. Shaqfeh, *"The shape stability of a lipid vesicle in a uniaxial extensional flow,"* J. Fluid Mech. **719**, 345 (2013).

[96] H. Zhao and E. S. G. Shaqfeh, *"The dynamics of a nondilute vesicle suspension in a simple shear flow,"* J. Fluid Mech. **725**, 709 (2013).

[97] P. M. Vlahovska, T. Podgorski, and C. Misbah, *"Vesicles and red blood cells in flow: From individual dynamics to rheology,"* Comptes Rendus Phys. **10**, 775 (2009).

[98] Y. Seol, W.-F. Hu, Y. Kim, and M.-C. Lai, *"An immersed boundary method for simulating vesicle dynamics in three dimensions,"* J. Comput. Phys. **322**, 125 (2016).

[99] A. Farutin, T. Piasecki, A. M. Słowicka, C. Misbah, E. Wajnryb, and M. L. Ekiel-Jeżewska, *"Dynamics of flexible fibers and vesicles in Poiseuille flow at low Reynolds number,"* Soft Matter **12**, 7307 (2016).

[100] C. Pozrikidis, *Introduction to Theoretical and Computational Fluid Dynamics*, 2nd ed. (Oxford University Press, New York, 2011).

[101] S. K. Veerapaneni, A. Rahimian, G. Biros, and D. Zorin, *"A fast algorithm for simulating vesicle flows in three dimensions,"* J. Comput. Phys. **230**, 5610 (2011).

[102] A. P. Spann, H. Zhao, and E. S. G. Shaqfeh, *"Loop subdivision surface boundary integral method simulations of vesicles at low reduced volume ratio in shear and extensional flow,"* Phys. Fluids **26**, 031902 (2014).

[103] A. Rahimian, S. K. Veerapaneni, D. Zorin, and G. Biros, *"Boundary integral method for the flow of vesicles with viscosity contrast in three dimensions,"* J. Comput. Phys. **298**, 766 (2015).

[104] P. Bagchi, in *Computational Hydrodynamics of Capsules and Biological Cells*, Chapman & Hall/CRC Mathematical and Computational Biology Series, edited by C. Pozrikidis (CRC Press, Boca Raton, 2010) pp. 35–70.

[105] D. A. Fedosov, B. Caswell, and G. E. Karniadakis, *"A Multiscale Red Blood Cell Model with Accurate Mechanics, Rheology, and Dynamics,"* Biophys. J. **98**, 2215 (2010).

[106] H. Noguchi and G. Gompper, *"Dynamics of fluid vesicles in shear flow: Effect of membrane viscosity and thermal fluctuations,"* Phys. Rev. E **72**, 011901 (2005).

[107] A. Farutin, T. Biben, and C. Misbah, *"3D numerical simulations of vesicle and inextensible capsule dynamics,"* J. Comput. Phys. **275**, 539 (2014).

[108] R. Skalak, A. Tozeren, R. P. Zarda, and S. Chien, *"Strain Energy Function of Red Blood Cell Membranes,"* Biophys. J. **13**, 245 (1973).

[109] H. Zhao, E. S. G. Shaqfeh, and V. Narsimhan, *"Shear-induced particle migration and margination in a cellular suspension,"* Phys. Fluids **24**, 011902 (2012).

[110] A. Guckenberger and S. Gekle, *"A boundary integral method with volume-changing objects for ultrasound-triggered margination of microbubbles,"* arXiv:1608.05196 [physics] (2017), arXiv:1608.05196 [physics].

[111] D. J. Steigmann, *"On the Relationship between the Cosserat and Kirchhoff-Love Theories of Elastic Shells,"* Math. Mech. Solids **4**, 275 (1999).

[112] R. A. Sauer and T. X. Duong, *"On the theoretical foundations of thin solid and liquid shells,"* Math. Mech. Solids , 1 (2015).

[113] C. K. Aidun and J. R. Clausen, *"Lattice-Boltzmann Method for Complex Flows,"* Annu. Rev. Fluid Mech. **42**, 439 (2010).

[114] J. L. McWhirter, H. Noguchi, and G. Gompper, *"Flow-induced clustering and alignment of vesicles and red blood cells in microcapillaries,"* Proc. Natl. Acad. Sci. **106**, 6039 (2009).

[115] J. L. McWhirter, H. Noguchi, and G. Gompper, *"Deformation and clustering of red blood cells in microcapillary flows,"* Soft Matter **7**, 10967 (2011).

[116] A. Lamura and G. Gompper, *"Dynamics and rheology of vesicle suspensions in wall-bounded shear flow,"* EPL Europhys. Lett. **102**, 28004 (2013).

[117] D. A. Fedosov, W. Pan, B. Caswell, G. Gompper, and G. E. Karniadakis, *"Predicting human blood viscosity in silico,"* Proc. Natl. Acad. Sci. **108**, 11772 (2011).

[118] D. A. Fedosov, B. Caswell, S. Suresh, and G. E. Karniadakis, *"Quantifying the biophysical characteristics of Plasmodium-falciparum-parasitized red blood cells in microcirculation,"* Proc. Natl. Acad. Sci. **108**, 35 (2011).

[119] D. A. Fedosov, J. Fornleitner, and G. Gompper, *"Margination of White Blood Cells in Microcapillary Flow,"* Phys. Rev. Lett. **108**, 028104 (2012).

[120] X. Li, A. S. Popel, and G. E. Karniadakis, *"Blood–plasma separation in Y-shaped bifurcating microfluidic channels: A dissipative particle dynamics simulation study,"* Phys. Biol. **9**, 026010 (2012).

[121] D. A. Fedosov and G. Gompper, *"White blood cell margination in microcirculation,"* Soft Matter **10**, 2961 (2014).

[122] K. Müller, D. A. Fedosov, and G. Gompper, *"Margination of micro- and nano-particles in blood flow and its*

effect on drug delivery," Sci. Rep. **4**, 4871 (2014).
[123] D. Katanov, G. Gompper, and D. A. Fedosov, *"Microvascular blood flow resistance: Role of red blood cell migration and dispersion,"* Microvasc. Res. **99**, 57 (2015).
[124] K. Lykov, X. Li, H. Lei, I. V. Pivkin, and G. E. Karniadakis, *"Inflow/Outflow Boundary Conditions for Particle-Based Blood Flow Simulations: Application to Arterial Bifurcations and Trees,"* PLOS Comput. Biol. **11**, e1004410 (2015).
[125] K. Müller, D. A. Fedosov, and G. Gompper, *"Understanding particle margination in blood flow – A step toward optimized drug delivery systems,"* Med. Eng. Phys. **38**, 2 (2016).
[126] A. Yazdani and G. E. Karniadakis, *"Sub-cellular modeling of platelet transport in blood flow through microchannels with constriction,"* Soft Matter **12**, 4339 (2016).
[127] R. M. MacMeccan, J. R. Clausen, G. P. Neitzel, and C. K. Aidun, *"Simulating deformable particle suspensions using a coupled lattice-Boltzmann and finite-element method,"* J. Fluid Mech. **618**, 13 (2009).
[128] J. R. Clausen and C. K. Aidun, *"Capsule dynamics and rheology in shear flow: Particle pressure and normal stress,"* Phys. Fluids **22**, 123302 (2010).
[129] J. R. Clausen, D. A. Reasor, and C. K. Aidun, *"The rheology and microstructure of concentrated non-colloidal suspensions of deformable capsules,"* J. Fluid Mech. **685**, 202 (2011).
[130] Z. Peng, R. J. Asaro, and Q. Zhu, *"Multiscale modelling of erythrocytes in Stokes flow,"* J. Fluid Mech. **686**, 299 (2011).
[131] C. Dupont, A.-V. Salsac, D. Barthès-Biesel, M. Vidrascu, and P. L. Tallec, *"Influence of bending resistance on the dynamics of a spherical capsule in shear flow,"* Phys. Fluids **27**, 051902 (2015).
[132] J. Sigüenza, S. Mendez, D. Ambard, F. Dubois, F. Jourdan, R. Mozul, and F. Nicoud, *"Validation of an immersed thick boundary method for simulating fluid–structure interactions of deformable membranes,"* J. Comput. Phys. **322**, 723 (2016).
[133] D.-V. Le and Z. Tan, *"Large deformation of liquid capsules enclosed by thin shells immersed in the fluid,"* J. Comput. Phys. **229**, 4097 (2010).
[134] M. Rahimi and M. Arroyo, *"Shape dynamics, lipid hydrodynamics, and the complex viscoelasticity of bilayer membranes,"* Phys. Rev. E **86**, 011932 (2012).
[135] M. M. Dupin, I. Halliday, C. M. Care, L. Alboul, and L. L. Munn, *"Modeling the flow of dense suspensions of deformable particles in three dimensions,"* Phys. Rev. E **75**, 066707 (2007).
[136] M. Dupin, I. Halliday, C. Care, and L. Munn, *"Lattice Boltzmann modelling of blood cell dynamics,"* Int. J. Comput. Fluid Dyn. **22**, 481 (2008).
[137] I. Cimrák, M. Gusenbauer, and T. Schrefl, *"Modelling and simulation of processes in microfluidic devices for biomedical applications,"* Comput. Math. Appl. **64**, 278 (2012).
[138] U. Seifert, *"The concept of effective tension for fluctuating vesicles,"* Z. Physik B - Condensed Matter **97**, 299 (1995).
[139] G. H. W. Lim, M. Wortis, and R. Mukhopadhyay, *"Stomatocyte–discocyte–echinocyte sequence of the human red blood cell: Evidence for the bilayer– couple hypothesis from membrane mechanics,"* Proc. Natl. Acad. Sci. **99**, 16766 (2002).
[140] M. N. Jaric, *Gaussian Fluctuations of Lipid Bilayer Vesicles: A Numerical Study*, Thesis, Simon Fraser University, Burnaby (2008).
[141] K. Khairy and J. Howard, *"Minimum-energy vesicle and cell shapes calculated using spherical harmonics parameterization,"* Soft Matter **7**, 2138 (2011).
[142] R. Mukhopadhyay, H. W. Gerald Lim, and M. Wortis, *"Echinocyte Shapes: Bending, Stretching, and Shear Determine Spicule Shape and Spacing,"* Biophys. J. **82**, 1756 (2002).
[143] J. W. Barrett, H. Garcke, and R. Nürnberg, *"Numerical computations of the dynamics of fluidic membranes and vesicles,"* Phys. Rev. E **92**, 052704 (2015).
[144] P. Bassereau, B. Sorre, and A. Lévy, *"Bending lipid membranes: Experiments after W. Helfrich's model,"* Adv. Colloid Interface Sci. **208**, 47 (2014).
[145] J. Li, G. Lykotrafitis, M. Dao, and S. Suresh, *"Cytoskeletal dynamics of human erythrocyte,"* Proc. Natl. Acad. Sci. **104**, 4937 (2007).
[146] D. Cordasco, A. Yazdani, and P. Bagchi, *"Comparison of erythrocyte dynamics in shear flow under different stress-free configurations,"* Phys. Fluids **26**, 041902 (2014).
[147] K.-i. Tsubota, S. Wada, and H. Liu, *"Elastic behavior of a red blood cell with the membrane's nonuniform natural state: Equilibrium shape, motion transition under shear flow, and elongation during tank-treading motion,"* Biomech. Model. Mechanobiol. **13**, 735 (2014).
[148] D. Cordasco and P. Bagchi, *"Dynamics of red blood cells in oscillating shear flow,"* J. Fluid Mech. **800**, 484 (2016).
[149] D. V. Le, *"Effect of bending stiffness on the deformation of liquid capsules enclosed by thin shells in shear flow,"* Phys. Rev. E **82**, 016318 (2010).
[150] R. Dimova, *"Recent developments in the field of bending rigidity measurements on membranes,"* Adv. Colloid Interface Sci. **208**, 225 (2014).
[151] J. F. Nagle, M. S. Jablin, S. Tristram-Nagle, and K. Akabori, *"What are the true values of the bending modulus of simple lipid bilayers?"* Chem. Phys. Lipids **185**, 3 (2015).
[152] D. Bochicchio and L. Monticelli, in *Advances in Biomembranes and Lipid Self-Assembly*, Vol. 23, edited by A. Iglič, C. V. Kulkarni, and M. Rappolt (Academic Press, Cambridge, 2016) pp. 117–143.
[153] S. Guido and G. Tomaiuolo, *"Microconfined flow behavior of red blood cells in vitro,"* Comptes Rendus Phys. **10**, 751 (2009).
[154] E. A. Evans, *"Bending elastic modulus of red blood cell membrane derived from buckling instability in micropipet aspiration tests,"* Biophys. J. **43**, 27 (1983).
[155] N. Mohandas and E. Evans, *"Mechanical Properties of the Red Cell Membrane in Relation to Molecular Structure and Genetic Defects,"* Annu. Rev. Biophys. Biomol. Struct. **23**, 787 (1994).
[156] F. J. Byfield, H. Aranda-Espinoza, V. G. Romanenko, G. H. Rothblat, and I. Levitan, *"Cholesterol Depletion Increases Membrane Stiffness of Aortic Endothelial Cells,"* Biophys. J. **87**, 3336 (2004).
[157] J.-B. Fournier and P. Galatola, *"Corrections to the Laplace law for vesicle aspiration in micropipettes and other confined geometries,"* Soft Matter **4**, 2463 (2008).
[158] D. E. Discher, D. H. Boal, and S. K. Boey, *"Simulations of the Erythrocyte Cytoskeleton at Large Deformation. II. Micropipette Aspiration,"* Biophys. J. **75**, 1584 (1998).
[159] Z. Peng, R. J. Asaro, and Q. Zhu, *"Multiscale simulation*

of erythrocyte membranes," Phys. Rev. E **81**, 031904 (2010).

[160] C. Dupont, P. Le Tallec, D. Barthès-Biesel, M. Vidrascu, and A. V. Salsac, *"Dynamics of a Spherical Capsule in a Planar Hyperbolic flow: Influence of bending Resistance,"* Procedia IUTAM IUTAM Symposium on Dynamics of Capsules, Vesicles and Cells in Flow (15-19 July 2014; Compiègne, France), **16**, 70 (2015).

[161] H. Noguchi, *"Anisotropic surface tension of buckled fluid membranes,"* Phys. Rev. E **83**, 061919 (2011).

[162] M. Hu, P. D. Iv, and M. Deserno, *"Determining the bending modulus of a lipid membrane by simulating buckling,"* J. Chem. Phys. **138**, 214110 (2013).

[163] M. Costa, I. Ghiran, C.-K. Peng, A. Nicholson-Weller, and A. L. Goldberger, *"Complex dynamics of human red blood cell flickering: Alterations with in vivo aging,"* Phys. Rev. E **78**, 020901 (2008).

[164] T. Betz, M. Lenz, J.-F. Joanny, and C. Sykes, *"ATP-dependent mechanics of red blood cells,"* Proc. Natl. Acad. Sci. **106**, 15320 (2009).

[165] Y. Park, C. A. Best, K. Badizadegan, R. R. Dasari, M. S. Feld, T. Kuriabova, M. L. Henle, A. J. Levine, and G. Popescu, *"Measurement of red blood cell mechanics during morphological changes,"* Proc. Natl. Acad. Sci. **107**, 6731 (2010).

[166] H. Byun, T. R. Hillman, J. M. Higgins, M. Diez-Silva, Z. Peng, M. Dao, R. R. Dasari, S. Suresh, and Y. Park, *"Optical measurement of biomechanical properties of individual erythrocytes from a sickle cell patient,"* Acta Biomater. **8**, 4130 (2012).

[167] H. Wennerström and U. Olsson, *"The undulation force; theoretical results versus experimental demonstrations,"* Adv. Colloid Interface Sci. **208**, 10 (2014).

[168] C. Minetti, V. Vitkova, F. Dubois, and I. Bivas, *"Digital holographic miscroscopy as a tool to study the thermal shape fluctuations of lipid vesicles,"* Opt. Lett. **41**, 1833 (2016).

[169] H. Turlier, D. A. Fedosov, B. Audoly, T. Auth, N. S. Gov, C. Sykes, J.-F. Joanny, G. Gompper, and T. Betz, *"Equilibrium physics breakdown reveals the active nature of red blood cell flickering,"* Nat. Phys. **12**, 513 (2016).

[170] M. C. Watson, E. G. Brandt, P. M. Welch, and F. L. H. Brown, *"Determining Biomembrane Bending Rigidities from Simulations of Modest Size,"* Phys. Rev. Lett. **109**, 028102 (2012).

[171] M. Deserno, K. Kremer, H. Paulsen, C. Peter, and F. Schmid, in *From Single Molecules to Nanoscopically Structured Materials*, Advances in Polymer Science No. 260, edited by T. Basché, K. Müllen, and M. Schmidt (Springer International Publishing, 2013) pp. 237–283.

[172] P. Tarazona, E. Chacón, and F. Bresme, *"Thermal fluctuations and bending rigidity of bilayer membranes,"* J. Chem. Phys. **139**, 094902 (2013).

[173] A. J. Sodt, R. M. Venable, E. Lyman, and R. W. Pastor, *"Nonadditive Compositional Curvature Energetics of Lipid Bilayers,"* Phys. Rev. Lett. **117**, 138104 (2016).

[174] J. P. Mills, L. Qie, M. Dao, C. T. Lim, and S. Suresh, *"Nonlinear elastic and viscoelastic deformation of the human red blood cell with optical tweezers,"* Mol. Cell. Biomech. **1**, 169 (2004).

[175] S. Suresh, J. Spatz, J. P. Mills, A. Micoulet, M. Dao, C. T. Lim, M. Beil, and T. Seufferlein, *"Connections between single-cell biomechanics and human disease states: Gastrointestinal cancer and malaria,"* Acta Biomater. **1**, 15 (2005).

[176] L. Scheffer, A. Bitler, E. Ben-Jacob, and R. Korenstein, *"Atomic force pulling: Probing the local elasticity of the cell membrane,"* Eur. Biophys. J. **30**, 83 (2001).

[177] M. Dao, J. Li, and S. Suresh, *"Molecularly based analysis of deformation of spectrin network and human erythrocyte,"* Mater. Sci. Eng. C Proceedings of the First TMS Symposium on Biological Materials Science, **26**, 1232 (2006).

[178] D. A. Fedosov, B. Caswell, and G. E. Karniadakis, *"Systematic coarse-graining of spectrin-level red blood cell models,"* Comput. Methods Appl. Mech. Eng. **199**, 1937 (2010).

[179] D. A. Reasor, J. R. Clausen, and C. K. Aidun, *"Coupling the lattice-Boltzmann and spectrin-link methods for the direct numerical simulation of cellular blood flow,"* Int. J. Numer. Methods Fluids **68**, 767 (2012).

[180] T. Krüger, D. Holmes, and P. V. Coveney, *"Deformability-based red blood cell separation in deterministic lateral displacement devices—A simulation study,"* Biomicrofluidics **8**, 054114 (2014).

[181] Z. Y. Luo and B. F. Bai, *"Dynamics of biconcave vesicles in a confined shear flow,"* Chem. Eng. Sci. **137**, 548 (2015).

[182] W. Hao, Z. Xu, C. Liu, and G. Lin, *"A fictitious domain method with a hybrid cell model for simulating motion of cells in fluid flow,"* J. Comput. Phys. **280**, 345 (2015).

[183] I. R. Suárez, C. Leidy, G. Téllez, G. Gay, and A. Gonzalez-Mancera, *"Slow Sedimentation and Deformability of Charged Lipid Vesicles,"* PLoS ONE **8**, e68309 (2013).

[184] V. Cristini, J. Bławzdziewicz, and M. Loewenberg, *"An Adaptive Mesh Algorithm for Evolving Surfaces: Simulations of Drop Breakup and Coalescence,"* J. Comput. Phys. **168**, 445 (2001).

[185] I. B. Bazhlekov, P. D. Anderson, and H. E. H. Meijer, *"Nonsingular boundary integral method for deformable drops in viscous flows,"* Phys. Fluids **16**, 1064 (2004).

[186] F. R. Cunha and M. Loewenberg, *"A study of emulsion expansion by a boundary integral method,"* Mech. Res. Commun. **30**, 639 (2003).

[187] S. L. G. de Oliveira, in *Computational Science and Its Applications – ICCSA 2012*, Lecture Notes in Computer Science No. 7333, edited by B. Murgante, O. Gervasi, S. Misra, N. Nedjah, A. M. A. C. Rocha, D. Taniar, and B. O. Apduhan (Springer Berlin Heidelberg, 2012) pp. 198–213.

[188] H. Noguchi and G. Gompper, *"Shape transitions of fluid vesicles and red blood cells in capillary flows,"* Proc. Natl. Acad. Sci. U. S. A. **102**, 14159 (2005).

[189] D. A. Fedosov, B. Caswell, and G. E. Karniadakis, in *Computational Hydrodynamics of Capsules and Biological Cells*, Chapman & Hall/CRC Mathematical and Computational Biology Series (CRC Press, 2010) pp. 183–218.

[190] A. Nans, N. Mohandas, and D. L. Stokes, *"Native Ultrastructure of the Red Cell Cytoskeleton by Cryo-Electron Tomography,"* Biophys. J. **101**, 2341 (2011).

[191] T. Omori, T. Ishikawa, D. Barthès-Biesel, A.-V. Salsac, J. Walter, Y. Imai, and T. Yamaguchi, *"Comparison between spring network models and continuum constitutive laws: Application to the large deformation of a capsule in shear flow,"* Phys. Rev. E **83**, 041918 (2011).

[192] S. Ramanujan and C. Pozrikidis, *"Deformation of liq-*

uid capsules enclosed by elastic membranes in simple shear flow: Large deformations and the effect of fluid viscosities," J. Fluid Mech. **361**, 117 (1998).

[193] J. Walter, A.-V. Salsac, D. Barthès-Biesel, and P. Le Tallec, *"Coupling of finite element and boundary integral methods for a capsule in a Stokes flow,"* Int. J. Numer. Methods Eng. **83**, 829 (2010).

[194] C. Pozrikidis, *"A spectral collocation method with triangular boundary elements,"* Engineering Analysis with Boundary Elements **30**, 315 (2006).

[195] Y. Wang and P. Dimitrakopoulos, *"A three-dimensional spectral boundary element algorithm for interfacial dynamics in Stokes flow,"* Phys. Fluids **18**, 082106 (2006).

[196] W. R. Dodson III and P. Dimitrakopoulos, *"Spindles, Cusps, and Bifurcation for Capsules in Stokes Flow,"* Phys. Rev. Lett. **101**, 208102 (2008).

[197] W. R. Dodson III and P. Dimitrakopoulos, *"Dynamics of strain-hardening and strain-softening capsules in strong planar extensional flows via an interfacial spectral boundary element algorithm for elastic membranes,"* J. Fluid Mech. **641**, 263 (2009).

[198] F. Cirak, M. Ortiz, and P. Schröder, *"Subdivision surfaces: A new paradigm for thin-shell finite-element analysis,"* Int. J. Numer. Methods Eng. **47**, 2039 (2000).

[199] E. Catmull and J. Clark, *"Recursively generated B-spline surfaces on arbitrary topological meshes,"* Comput.-Aided Des. **10**, 350 (1978).

[200] D.-V. Le and S. T. Wong, *"A front-tracking method with Catmull–Clark subdivision surfaces for studying liquid capsules enclosed by thin shells in shear flow,"* J. Comput. Phys. **230**, 3538 (2011).

[201] C. T. Loop, *Smooth Subdivision Surfaces Based on Triangles*, Master thesis, University of Utah, Utah, USA (1987).

[202] P.-O. Persson, M. J. Aftosmis, and R. Haimes, in *Proceedings of the 15th International Meshing Roundtable*, edited by P. P. Pébay (Springer Berlin Heidelberg, 2006) pp. 375–392.

[203] D.-V. Le, *"Subdivision elements for large deformation of liquid capsules enclosed by thin shells,"* Comput. Methods Appl. Mech. Eng. **199**, 2622 (2010).

[204] J. Gounley, G. Boedec, M. Jaeger, and M. Leonetti, *"Influence of surface viscosity on droplets in shear flow,"* J. Fluid Mech. **791**, 464 (2016).

[205] W.-X. Huang, C. B. Chang, and H. J. Sung, *"Three-dimensional simulation of elastic capsules in shear flow by the penalty immersed boundary method,"* J. Comput. Phys. **231**, 3340 (2012).

[206] S. Kessler, R. Finken, and U. Seifert, *"Swinging and tumbling of elastic capsules in shear flow,"* J. Fluid Mech. **605**, 207 (2008).

[207] J. B. Freund and H. Zhao, in *Computational Hydrodynamics of Capsules and Biological Cells*, Chapman & Hall/CRC Mathematical and Computational Biology Series, edited by C. Pozrikidis (CRC Press, Boca Raton, 2010) pp. 71–111.

[208] A. Rahimian, I. Lashuk, S. Veerapaneni, A. Chandramowlishwaran, D. Malhotra, L. Moon, R. Sampath, A. Shringarpure, J. Vetter, R. Vuduc, D. Zorin, and G. Biros, in *Proceedings of the 2010 ACM/IEEE International Conference for High Performance Computing, Networking, Storage and Analysis* (IEEE Computer Society, New Orleans, 2010).

[209] S. Veerapaneni, *"Integral equation methods for vesicle electrohydrodynamics in three dimensions,"* J. Comput. Phys. **326**, 278 (2016).

[210] H. Zhou and C. Pozrikidis, *"Deformation of liquid capsules with incompressible interfaces in simple shear flow,"* J. Fluid Mech. **283**, 175 (1995).

[211] E. Lac, D. Barthès-Biesel, N. A. Pelekasis, and J. Tsamopoulos, *"Spherical capsules in three-dimensional unbounded Stokes flows: Effect of the membrane constitutive law and onset of buckling,"* J. Fluid Mech. **516**, 303 (2004).

[212] D. Barthès-Biesel, J. Walter, and A.-V. Salsac, in *Computational Hydrodynamics of Capsules and Biological Cells*, Chapman & Hall/CRC Mathematical and Computational Biology Series, edited by C. Pozrikidis (CRC Press, Boca Raton, 2010) pp. 35–70.

[213] R. Rangarajan and H. Gao, *"A finite element method to compute three-dimensional equilibrium configurations of fluid membranes: Optimal parameterization, variational formulation and applications,"* J. Comput. Phys. **297**, 266 (2015).

[214] E. Lac, A. Morel, and D. Barthès-Biesel, *"Hydrodynamic interaction between two identical capsules in simple shear flow,"* J. Fluid Mech. **573**, 149 (2007).

[215] T. Biben, K. Kassner, and C. Misbah, *"Phase-field approach to three-dimensional vesicle dynamics,"* Phys. Rev. E **72**, 041921 (2005).

[216] Q. Du and J. Zhang, *"Adaptive Finite Element Method for a Phase Field Bending Elasticity Model of Vesicle Membrane Deformations,"* SIAM J. Sci. Comput. **30**, 1634 (2008).

[217] S. K. Veerapaneni, D. Gueyffier, D. Zorin, and G. Biros, *"A boundary integral method for simulating the dynamics of inextensible vesicles suspended in a viscous fluid in 2D,"* J. Comput. Phys. **228**, 2334 (2009).

[218] B. Kaoui, G. Biros, and C. Misbah, *"Why Do Red Blood Cells Have Asymmetric Shapes Even in a Symmetric Flow?"* Phys. Rev. Lett. **103**, 188101 (2009).

[219] Z. Y. Luo, F. Xu, T. J. Lu, and B. F. Bai, *"Direct Numerical Simulation of Single Leukocyte Deformation in Microchannel Flow for Disease Diagnosis,"* J. Med. Syst. **35**, 869 (2010).

[220] D. Salac and M. Miksis, *"A level set projection model of lipid vesicles in general flows,"* J. Comput. Phys. **230**, 8192 (2011).

[221] A. Laadhari, P. Saramito, and C. Misbah, *"Vesicle tumbling inhibited by inertia,"* Phys. Fluids **24**, 031901 (2012).

[222] A. Laadhari, P. Saramito, and C. Misbah, *"Computing the dynamics of biomembranes by combining conservative level set and adaptive finite element methods,"* J. Comput. Phys. **263**, 328 (2014).

[223] A. Laadhari, P. Saramito, and C. Misbah, *"An adaptive finite element method for the modeling of the equilibrium of red blood cells,"* Int. J. Numer. Meth. Fluids **80**, 397 (2016).

[224] W. Marth, S. Aland, and A. Voigt, *"Margination of white blood cells: A computational approach by a hydrodynamic phase field model,"* J. Fluid Mech. **790**, 389 (2016).

[225] G. Ghigliotti, T. Biben, and C. Misbah, *"Rheology of a dilute two-dimensional suspension of vesicles,"* J. Fluid Mech. **653**, 489 (2010).

[226] Y. Sui, Y. Chew, P. Roy, X. Chen, and H. Low, *"Transient deformation of elastic capsules in shear flow: Effect of membrane bending stiffness,"* Phys. Rev. E **75**, 066301

(2007).
[227] J. B. Freund, *"Leukocyte margination in a model microvessel,"* Phys. Fluids **19**, 023301 (2007).
[228] J. S. Sohn, Y.-H. Tseng, S. Li, A. Voigt, and J. S. Lowengrub, *"Dynamics of multicomponent vesicles in a viscous fluid,"* J. Comput. Phys. **229**, 119 (2010).
[229] A. Rahimian, S. K. Veerapaneni, and G. Biros, *"Dynamic simulation of locally inextensible vesicles suspended in an arbitrary two-dimensional domain, a boundary integral method,"* Journal of Computational Physics **229**, 6466 (2010).
[230] R. Trozzo, G. Boedec, M. Leonetti, and M. Jaeger, *"Axisymmetric Boundary Element Method for vesicles in a capillary,"* J. Comput. Phys. **289**, 62 (2015).
[231] H.-H. Boltz and J. Kierfeld, *"Shapes of sedimenting soft elastic capsules in a viscous fluid,"* Phys. Rev. E **92**, 033003 (2015).
[232] S. K. Veerapaneni, D. Gueyffier, G. Biros, and D. Zorin, *"A numerical method for simulating the dynamics of 3D axisymmetric vesicles suspended in viscous flows,"* J. Comput. Phys. **228**, 7233 (2009).
[233] J. Sohn, S. Li, X. Li, and J. S. Lowengrub, *"Axisymmetric multicomponent vesicles: A comparison of hydrodynamic and geometric models,"* Int. J. Numer. Meth. Biomed. Engng. **28**, 346 (2012).
[234] Q. Du, C. Liu, and X. Wang, *"A phase field approach in the numerical study of the elastic bending energy for vesicle membranes,"* J. Comput. Phys. **198**, 450 (2004).
[235] A. Rosolen, C. Peco, and M. Arroyo, *"An adaptive meshfree method for phase-field models of biomembranes. Part I: Approximation with maximum-entropy basis functions,"* J. Comput. Phys. **249**, 303 (2013).
[236] J. Lowengrub, J. Allard, and S. Aland, *"Numerical simulation of endocytosis: Viscous flow driven by membranes with non-uniformly distributed curvature-inducing molecules,"* J. Comput. Phys. **309**, 112 (2016).
[237] M. Kraus, W. Wintz, U. Seifert, and R. Lipowsky, *"Fluid Vesicles in Shear Flow,"* Phys. Rev. Lett. **77**, 3685 (1996).
[238] T. Krüger, F. Varnik, and D. Raabe, *"Efficient and accurate simulations of deformable particles immersed in a fluid using a combined immersed boundary lattice Boltzmann finite element method,"* Comput. Math. Appl. **61**, 3485 (2011).
[239] M. Meyer, M. Desbrun, P. Schröder, and A. H. Barr, in *Visualization and Mathematics III*, Mathematics and Visualization No. 3, edited by H.-C. Hege and K. Polthier (Springer, Berlin, Heidelberg, 2003) pp. 35–57.
[240] Y. Kantor and D. R. Nelson, *"Phase transitions in flexible polymeric surfaces,"* Phys. Rev. A **36**, 4020 (1987).
[241] G. Gompper and D. M. Kroll, *"Random Surface Discretizations and the Renormalization of the Bending Rigidity,"* J. Phys. Fr. **6**, 1305 (1996).
[242] S. Komura, K. Tamura, and T. Kato, *"Buckling of spherical shells adhering onto a rigid substrate,"* Eur. Phys. J. E **18**, 343 (2005).
[243] J. Li, M. Dao, C. T. Lim, and S. Suresh, *"Spectrin-Level Modeling of the Cytoskeleton and Optical Tweezers Stretching of the Erythrocyte,"* Biophys. J. **88**, 3707 (2005).
[244] I. V. Pivkin and G. E. Karniadakis, *"Accurate Coarse-Grained Modeling of Red Blood Cells,"* Phys. Rev. Lett. **101**, 118105 (2008).
[245] W. Pan, B. Caswell, and G. E. Karniadakis, *"A low-dimensional model for the red blood cell,"* Soft Matter **6**, 4366 (2010).
[246] W. Pan, D. A. Fedosov, B. Caswell, and G. E. Karniadakis, *"Predicting dynamics and rheology of blood flow: A comparative study of multiscale and low-dimensional models of red blood cells,"* Microvasc. Res. **82**, 163 (2011).
[247] R. Kusters, T. van der Heijden, B. Kaoui, J. Harting, and C. Storm, *"Forced transport of deformable containers through narrow constrictions,"* Phys. Rev. E **90**, 033006 (2014).
[248] D. A. Fedosov, M. Peltomäki, and G. Gompper, *"Deformation and dynamics of red blood cells in flow through cylindrical microchannels,"* Soft Matter **10**, 4258 (2014).
[249] Z. Zhang, E. Henry, G. Gompper, and D. A. Fedosov, *"Behavior of rigid and deformable particles in deterministic lateral displacement devices with different post shapes,"* J. Chem. Phys. **143**, 243145 (2015).
[250] M. Mehrabadi, D. N. Ku, and C. K. Aidun, *"Effects of shear rate, confinement, and particle parameters on margination in blood flow,"* Phys. Rev. E **93**, 023109 (2016).
[251] A. P. Spann, J. E. Campbell, S. R. Fitzgibbon, A. Rodriguez, A. P. Cap, L. H. Blackbourne, and E. S. G. Shaqfeh, *"The Effect of Hematocrit on Platelet Adhesion: Experiments and Simulations,"* Biophys. J. **111**, 577 (2016).
[252] H. Noguchi and G. Gompper, *"Fluid Vesicles with Viscous Membranes in Shear Flow,"* Phys. Rev. Lett. **93**, 258102 (2004).
[253] H. Noguchi and G. Gompper, *"Swinging and Tumbling of Fluid Vesicles in Shear Flow,"* Phys. Rev. Lett. **98**, 128103 (2007).
[254] J. L. McWhirter, H. Noguchi, and G. Gompper, *"Ordering and arrangement of deformed red blood cells in flow through microcapillaries,"* New J. Phys. **14**, 085026 (2012).
[255] G. Xu, *"Convergence of discrete Laplace-Beltrami operators over surfaces,"* Comput. Math. Appl. **48**, 347 (2004).
[256] M. Botsch, M. Pauly, C. Rossl, S. Bischoff, and L. Kobbelt, in *ACM SIGGRAPH 2006 Courses*, SIGGRAPH '06 (ACM, New York, 2006).
[257] T. D. Gatzke and C. M. Grimm, *"Estimating curvature on triangular meshes,"* Int. J. Shape Model. **12**, 1 (2006).
[258] O. Sorkine, *"Differential Representations for Mesh Processing,"* Comput. Graph. Forum **25**, 789 (2006).
[259] K. Hildebrandt, K. Polthier, and M. Wardetzky, *"On the convergence of metric and geometric properties of polyhedral surfaces,"* Geom. Dedicata **123**, 89 (2007).
[260] M. Wardetzky, S. Mathur, F. Kälberer, and E. Grinspun, in *SGP '07 Proceedings of the Fifth Eurographics Symposium on Geometry Processing*, SGP '07, edited by A. Belyaev and M. Garland (Eurographics Association, Barcelona, 2007) pp. 33–37.
[261] M. Belkin, J. Sun, and Y. Wang, in *SCG '08: Proceedings of the Twenty-Fourth Annual Symposium on Computational Geometry* (ACM, Maryland, 2008) pp. 278–287.
[262] J. M. Sullivan, in *Discrete Differential Geometry*, Oberwolfach Seminars No. 38, edited by A. I. Bobenko, J. M. Sullivan, P. Schröder, and G. M. Ziegler (Birkhäuser Basel, 2008) pp. 175–188.
[263] M. Wardetzky, in *Discrete Differential Geometry*, Oberwolfach Seminars No. 38, edited by A. I. Bobenko, J. M.

Sullivan, P. Schröder, and G. M. Ziegler (Birkhäuser Basel, 2008) pp. 275–286.
[264] M. Reuter, S. Biasotti, D. Giorgi, G. Patanè, and M. Spagnuolo, *"Discrete Laplace–Beltrami operators for shape analysis and segmentation,"* Comput. Graph. **33**, 381 (2009).
[265] J.-Y. Wu, M.-H. Chi, and S.-G. Chen, *"A local tangential lifting differential method for triangular meshes,"* Math. Comput. Simul. **80**, 2386 (2010).
[266] M. Alexa and M. Wardetzky, in *SIGGRAPH '11* (ACM, New York, 2011) pp. 102:1–102:10.
[267] X. Yang and J. Zheng, *"Curvature tensor computation by piecewise surface interpolation,"* Comput.-Aided Des. **45**, 1639 (2013).
[268] S.-G. Chen, M.-H. Chi, and J.-Y. Wu, *"High-Order Algorithms for Laplace–Beltrami Operators and Geometric Invariants over Curved Surfaces,"* J. Sci. Comput. **65**, 839 (2015).
[269] X. Li, G. Xu, and Y. J. Zhang, *"Localized discrete Laplace–Beltrami operator over triangular mesh,"* Comput. Aided Geom. Des. **39**, 67 (2015).
[270] G. Boedec, M. Jaeger, and M. Leonetti, *"Settling of a vesicle in the limit of quasispherical shapes,"* J. Fluid Mech. **690**, 227 (2012).
[271] A. Farutin and C. Misbah, *"Squaring, Parity Breaking, and S Tumbling of Vesicles under Shear Flow,"* Phys. Rev. Lett. **109**, 248106 (2012).
[272] S. Bogner, U. Rüde, and J. Harting, *"Curvature estimation from a volume-of-fluid indicator function for the simulation of surface tension and wetting with a free-surface lattice Boltzmann method,"* Phys. Rev. E **93**, 043302 (2016).
[273] F. Fraternali, I. Farina, and G. Carpentieri, *"A discrete-to-continuum approach to the curvatures of membrane networks and parametric surfaces,"* Mech. Res. Commun. **56**, 18 (2014).
[274] A. Z. Zinchenko, M. A. Rother, and R. H. Davis, *"A novel boundary-integral algorithm for viscous interaction of deformable drops,"* Phys. Fluids **9**, 1493 (1997).
[275] A. Farutin and C. Misbah, *"Symmetry breaking and cross-streamline migration of three-dimensional vesicles in an axial Poiseuille flow,"* Phys. Rev. E **89**, 042709 (2014).
[276] A. Farutin and C. Misbah, *"Analytical and Numerical Study of Three Main Migration Laws for Vesicles Under Flow,"* Phys. Rev. Lett. **110**, 108104 (2013).
[277] G. Prado, A. Farutin, C. Misbah, and L. Bureau, *"Viscoelastic Transient of Confined Red Blood Cells,"* Biophys. J. **108**, 2126 (2015).
[278] A. Z. K. Yazdani, R. M. Kalluri, and P. Bagchi, *"Tank-treading and tumbling frequencies of capsules and red blood cells,"* Phys. Rev. E **83**, 046305 (2011).
[279] A. Yazdani and P. Bagchi, *"Influence of membrane viscosity on capsule dynamics in shear flow,"* J. Fluid Mech. **718**, 569 (2013).
[280] M. Zhao and P. Bagchi, *"Dynamics of microcapsules in oscillating shear flow,"* Phys. Fluids **23**, 111901 (2011).
[281] D. Cordasco and P. Bagchi, *"Orbital drift of capsules and red blood cells in shear flow,"* Phys. Fluids **25**, 091902 (2013).
[282] D. Cordasco and P. Bagchi, *"Intermittency and synchronized motion of red blood cell dynamics in shear flow,"* J. Fluid Mech. **759**, 472 (2014).
[283] K. Vahidkhah, S. L. Diamond, and P. Bagchi, *"Platelet Dynamics in Three-Dimensional Simulation of Whole Blood,"* Biophys. J. **106**, 2529 (2014).
[284] K. Vahidkhah and P. Bagchi, *"Microparticle shape effects on margination, near-wall dynamics and adhesion in a three-dimensional simulation of red blood cell suspension,"* Soft Matter **11**, 2097 (2015).
[285] K. Vahidkhah, P. Balogh, and P. Bagchi, *"Flow of Red Blood Cells in Stenosed Microvessels,"* Sci. Rep. **6**, 28194 (2016).
[286] S. Jin, R. R. Lewis, and D. West, *"A comparison of algorithms for vertex normal computation,"* Vis. Comput. **21**, 71 (2005).
[287] W. Bosch, *"On the computation of derivatives of Legendre functions,"* Phys. Chem. Earth Part Solid Earth Geod. **25**, 655 (2000).
[288] E. Kolahdouz and D. Salac, *"Electrohydrodynamics of Three-Dimensional Vesicles: A Numerical Approach,"* SIAM J. Sci. Comput. **37**, B473 (2015).
[289] S. S. Rao, *The Finite Element Method in Engineering*, 4th ed. (Butterworth-Heinemann, Boston, 2005).
[290] J. Barrett, H. Garcke, and R. Nürnberg, *"Finite element approximation for the dynamics of asymmetric fluidic biomembranes,"* Math. Comput. **86**, 1037 (2016).
[291] K. Deckelnick, J. Katz, and F. Schieweck, *"A C^1-finite element method for the Willmore flow of two-dimensional graphs,"* Math. Comput. **84**, 2617 (2015).
[292] R. E. Rusu, *"An algorithm for the elastic flow of surfaces,"* Interfaces Free Boundaries **7**, 229 (2005).
[293] J. W. Barrett, H. Garcke, and R. Nürnberg, *"A stable numerical method for the dynamics of fluidic membranes,"* Numer. Math. **134**, 783 (2016).
[294] D. S. Rodrigues, R. F. Ausas, F. Mut, and G. C. Buscaglia, *"A semi-implicit finite element method for viscous lipid membranes,"* J. Comput. Phys. **298**, 565 (2015).
[295] A. Bonito, R. H. Nochetto, and M. Sebastian Pauletti, *"Parametric FEM for geometric biomembranes,"* Journal of Computational Physics **229**, 3171 (2010).
[296] A. Bonito, R. H. Nochetto, and M. S. Pauletti, *"Dynamics of Biomembranes: Effect of the Bulk Fluid,"* Math. Model. Nat. Phenom. **6**, 25 (2011).
[297] H. J. Deuling and W. Helfrich, *"Red blood cell shapes as explained on the basis of curvature elasticity,"* Biophys. J. **16**, 861 (1976).
[298] M. G. Blyth and C. Pozrikidis, *"Solution space of axisymmetric capsules enclosed by elastic membranes,"* Eur. J. Mech. - ASolids **23**, 877 (2004).
[299] K. Khairy, J. Foo, and J. Howard, *"Shapes of Red Blood Cells: Comparison of 3D Confocal Images with the Bilayer-Couple Model,"* Cell. Mol. Bioeng. **1**, 173 (2008).
[300] K. A. Brakke, *"The Surface Evolver,"* Exp. Math. **1**, 141 (1992).
[301] P. Ziherl and S. Svetina, *"Nonaxisymmetric phospholipid vesicles: Rackets, boomerangs, and starfish,"* Europhys. Lett. EPL **70**, 690 (2005).
[302] A. Sakashita, N. Urakami, P. Ziherl, and M. Imai, *"Three-dimensional analysis of lipid vesicle transformations,"* Soft Matter **8**, 8569 (2012).
[303] V. Heinrich, S. Svetina, and B. Žekš, *"Nonaxisymmetric vesicle shapes in a generalized bilayer-couple model and the transition between oblate and prolate axisymmetric shapes,"* Phys. Rev. E **48**, 3112 (1993).
[304] U. Seifert, *"Fluid membranes in hydrodynamic flow fields: Formalism and an application to fluctuating quasispheri-*

cal vesicles in shear flow," Eur. Phys. J. B **8**, 405 (1999).
[305] L. Miao, M. A. Lomholt, and J. Kleis, *"Dynamics of shape fluctuations of quasi-spherical vesicles revisited,"* Eur. Phys. J. E **9**, 143 (2002).
[306] A. Daddi-Moussa-Ider, A. Guckenberger, and S. Gekle, *"Particle mobility between two planar elastic membranes: Brownian motion and membrane deformation,"* Phys. Fluids **28**, 071903 (2016).
[307] A. Daddi-Moussa-Ider and S. Gekle, *"Hydrodynamic interaction between particles near elastic interfaces,"* J. Chem. Phys. **145**, 014905 (2016).
[308] A. Daddi-Moussa-Ider, M. Lisicki, and S. Gekle, *"Mobility of an axisymmetric particle near an elastic interface,"* J. Fluid Mech. **811**, 210 (2017).
[309] A. Daddi-Moussa-Ider and S. Gekle, *"Hydrodynamic mobility of a solid particle near a spherical elastic membrane: Axisymmetric motion,"* Phys. Rev. E **95**, 013108 (2017).
[310] J. Dupire, M. Abkarian, and A. Viallat, *"Chaotic Dynamics of Red Blood Cells in a Sinusoidal Flow,"* Phys. Rev. Lett. **104**, 168101 (2010).
[311] O. Aouane, M. Thiébaud, A. Benyoussef, C. Wagner, and C. Misbah, *"Vesicle dynamics in a confined Poiseuille flow: From steady state to chaos,"* Phys. Rev. E **90**, 033011 (2014).
[312] T. W. Secomb, R. Skalak, N. Özkaya, and J. F. Gross, *"Flow of axisymmetric red blood cells in narrow capillaries,"* J. Fluid Mech. **163**, 405 (1986).
[313] X. Li and K. Sarkar, *"Front tracking simulation of deformation and buckling instability of a liquid capsule enclosed by an elastic membrane,"* J. Comput. Phys. **227**, 4998 (2008).
[314] S. H. Bryngelson and J. B. Freund, *"Buckling and its effect on the confined flow of a model capsule suspension,"* Rheol. Acta **55**, 451 (2016).
[315] S. Kessler, R. Finken, and U. Seifert, *"Elastic capsules in shear flow: Analytical solutions for constant and time-dependent shear rates,"* Eur. Phys. J. E **29**, 399 (2009).
[316] H. Noguchi, *"Dynamic modes of red blood cells in oscillatory shear flow,"* Phys. Rev. E **81**, 061920 (2010).
[317] A. Farutin and C. Misbah, *"Rheology of vesicle suspensions under combined steady and oscillating shear flows,"* J. Fluid Mech. **700**, 362 (2012).
[318] D. Matsunaga, Y. Imai, T. Yamaguchi, and T. Ishikawa, *"Deformation of a spherical capsule under oscillating shear flow,"* J. Fluid Mech. **762**, 288 (2015).
[319] L. Zhu, J. Rabault, and L. Brandt, *"The dynamics of a capsule in a wall-bounded oscillating shear flow,"* Phys. Fluids **27**, 071902 (2015).
[320] G. Boedec, M. Jaeger, and M. Leonetti, *"Sedimentation-induced tether on a settling vesicle,"* Phys. Rev. E **88**, 010702 (2013).
[321] J. Gounley and Y. Peng, *"Response and Recovery Times of Elastic and Viscoelastic Capsules in Shear Flow,"* Commun. Comput. Phys. **17**, 1151 (2015).
[322] J. B. Freund, *"The flow of red blood cells through a narrow spleen-like slit,"* Phys. Fluids **25**, 110807 (2013).
[323] L. Zhu, C. Rorai, D. Mitra, and L. Brandt, *"A microfluidic device to sort capsules by deformability: A numerical study,"* Soft Matter **10**, 7705 (2014).
[324] P. R. Zarda, S. Chien, and R. Skalak, *"Elastic deformations of red blood cells,"* J. Biomech. **10**, 211 (1977).
[325] C. Misbah, *"Vacillating Breathing and Tumbling of Vesicles under Shear Flow,"* Phys. Rev. Lett. **96**, 028104 (2006).
[326] R. Finken, S. Kessler, and U. Seifert, *"Micro-capsules in shear flow,"* J. Phys. Condens. Matter **23**, 184113 (2011).
[327] P. M. Vlahovska, Y.-N. Young, G. Danker, and C. Misbah, *"Dynamics of a non-spherical microcapsule with incompressible interface in shear flow,"* J. Fluid Mech. **678**, 221 (2011).
[328] R. Tran-Son-Tay, S. P. Sutera, and P. R. Rao, *"Determination of red blood cell membrane viscosity from rheoscopic observations of tank-treading motion,"* Biophys. J. **46**, 65 (1984).
[329] M. Abkarian, M. Faivre, and A. Viallat, *"Swinging of Red Blood Cells under Shear Flow,"* Phys. Rev. Lett. **98**, 188302 (2007).
[330] A. Z. K. Yazdani and P. Bagchi, *"Phase diagram and breathing dynamics of a single red blood cell and a biconcave capsule in dilute shear flow,"* Phys. Rev. E **84**, 026314 (2011).
[331] T. M. Fischer and R. Korzeniewski, *"Angle of Inclination of Tank-Treading Red Cells: Dependence on Shear Rate and Suspending Medium,"* Biophys. J. **108**, 1352 (2015).
[332] M. Laumann, P. Bauknecht, S. Gekle, D. Kienle, and W. Zimmermann, *"Cross-stream migration of asymmetric particles driven by oscillating shear,"* Europhys. Lett. **117**, 44001 (2017).
[333] A. Farutin and C. Misbah, *"Symmetry breaking of vesicle shapes in Poiseuille flow,"* Phys. Rev. E **84**, 011902 (2011).
[334] G. Danker, P. M. Vlahovska, and C. Misbah, *"Vesicles in Poiseuille Flow,"* Phys. Rev. Lett. **102**, 148102 (2009).
[335] G. Coupier, A. Farutin, C. Minetti, T. Podgorski, and C. Misbah, *"Shape Diagram of Vesicles in Poiseuille Flow,"* Phys. Rev. Lett. **108**, 178106 (2012).
[336] M. Abkarian, M. Faivre, R. Horton, K. Smistrup, C. A. Best-Popescu, and H. A. Stone, *"Cellular-scale hydrodynamics,"* Biomed. Mater. **3**, 034011 (2008).
[337] G. Tomaiuolo, L. Lanotte, G. Ghigliotti, C. Misbah, and S. Guido, *"Red blood cell clustering in Poiseuille microcapillary flow,"* Phys. Fluids **24**, 051903 (2012).
[338] M. Brust, O. Aouane, M. Thiébaud, D. Flormann, C. Verdier, L. Kaestner, M. W. Laschke, H. Selmi, A. Benyoussef, T. Podgorski, G. Coupier, C. Misbah, and C. Wagner, *"The plasma protein fibrinogen stabilizes clusters of red blood cells in microcapillary flows,"* Sci. Rep. **4**, 4348 (2014).
[339] S. H. Bryngelson and J. B. Freund, *"Capsule-train stability,"* Phys. Rev. Fluids **1**, 033201 (2016).
[340] D. A. Fedosov, B. Caswell, A. S. Popel, and G. E. Karniadakis, *"Blood Flow and Cell-Free Layer in Microvessels,"* Microcirculation **17**, 615 (2010).
[341] J. B. Freund and M. M. Orescanin, *"Cellular flow in a small blood vessel,"* J. Fluid Mech. **671**, 466 (2011).
[342] H. Lei, D. A. Fedosov, B. Caswell, and G. E. Karniadakis, *"Blood flow in small tubes: Quantifying the transition to the non-continuum regime,"* J. Fluid Mech. **722**, 214 (2013).
[343] J. B. Freund and B. Shapiro, *"Transport of particles by magnetic forces and cellular blood flow in a model microvessel,"* Phys. Fluids **24**, 051904 (2012).
[344] H. Zhao and E. S. G. Shaqfeh, *"Shear-induced platelet margination in a microchannel,"* Phys. Rev. E **83**, 061924 (2011).
[345] D. A. Reasor, M. Mehrabadi, D. N. Ku, and C. K. Aidun, *"Determination of Critical Parameters in Platelet*

Margination," Ann. Biomed. Eng. **41**, 238 (2012).
[346] N. Takeishi, Y. Imai, K. Nakaaki, T. Yamaguchi, and T. Ishikawa, *"Leukocyte margination at arteriole shear rate,"* Physiol. Rep. **2**, e12037 (2014).
[347] S. Fitzgibbon, A. P. Spann, Q. M. Qi, and E. S. G. Shaqfeh, *"In Vitro Measurement of Particle Margination in the Microchannel Flow: Effect of Varying Hematocrit,"* Biophys. J. **108**, 2601 (2015).
[348] S. Gekle, *"Strongly Accelerated Margination of Active Particles in Blood Flow,"* Biophys. J. **110**, 514 (2016).
[349] T. Krüger, *"Effect of tube diameter and capillary number on platelet margination and near-wall dynamics,"* Rheol. Acta **55**, 511 (2016).
[350] C. Bächer, L. Schrack, and S. Gekle, *"Clustering of microscopic particles in constricted blood flow,"* Phys. Rev. Fluids **2**, 013102 (2017).
[351] H. H. Lipowsky, *"In vivo studies of blood rheology in the microcirculation in an in vitro world: Past, present and future,"* Biorheology **50**, 3 (2013).
[352] A. Kumar and M. D. Graham, *"Segregation by membrane rigidity in flowing binary suspensions of elastic capsules,"* Phys. Rev. E **84**, 066316 (2011).
[353] A. Kumar and M. D. Graham, *"Mechanism of Margination in Confined Flows of Blood and Other Multicomponent Suspensions,"* Phys. Rev. Lett. **109**, 108102 (2012).
[354] A. Kumar, R. G. Henríquez Rivera, and M. D. Graham, *"Flow-induced segregation in confined multicomponent suspensions: Effects of particle size and rigidity,"* J. Fluid Mech. **738**, 423 (2014).
[355] D. Matsunaga, Y. Imai, T. Omori, T. Ishikawa, and T. Yamaguchi, *"A full GPU implementation of a numerical method for simulating capsule suspensions,"* J. Biomech. Sci. Eng. **9**, 14-00039 (2014).
[356] E. Lac and D. Barthès-Biesel, *"Pairwise interaction of capsules in simple shear flow: Three-dimensional effects,"* Phys. Fluids **20**, 040801 (2008).
[357] S. K. Doddi and P. Bagchi, *"Effect of inertia on the hydrodynamic interaction between two liquid capsules in simple shear flow,"* Int. J. Multiph. Flow **34**, 375 (2008).
[358] D.-V. Le and K.-H. Chiam, *"Hydrodynamic interaction between two nonspherical capsules in shear flow,"* Phys. Rev. E **84**, 056322 (2011).
[359] T. Krüger, B. Kaoui, and J. Harting, *"Interplay of inertia and deformability on rheological properties of a suspension of capsules,"* J. Fluid Mech. **751**, 725 (2014).
[360] G. Ghigliotti, H. Selmi, L. E. Asmi, and C. Misbah, *"Why and how does collective red blood cells motion occur in the blood microcirculation?"* Phys. Fluids **24**, 101901 (2012).
[361] Z. Shen, G. Coupier, B. Kaoui, B. Polack, J. Harting, C. Misbah, and T. Podgorski, *"Inversion of hematocrit partition at microfluidic bifurcations,"* Microvasc. Res. **105**, 40 (2016).
[362] M. Thiébaud and C. Misbah, *"Rheology of a vesicle suspension with finite concentration: A numerical study,"* Phys. Rev. E **88**, 062707 (2013).
[363] M. Thiébaud, Z. Shen, J. Harting, and C. Misbah, *"Prediction of Anomalous Blood Viscosity in Confined Shear Flow,"* Phys. Rev. Lett. **112**, 238304 (2014).
[364] B. Quaife and G. Biros, *"High-order Adaptive Time Stepping for Vesicle Suspensions with Viscosity Contrast,"* Procedia IUTAM **16**, 89 (2015).
[365] B. Quaife and G. Biros, *"Adaptive time stepping for vesicle suspensions,"* J. Comput. Phys. **306**, 478 (2016).
[366] T. Krüger, M. Gross, D. Raabe, and F. Varnik, *"Crossover from tumbling to tank-treading-like motion in dense simulated suspensions of red blood cells,"* Soft Matter **9**, 9008 (2013).
[367] N. Takeishi, Y. Imai, T. Yamaguchi, and T. Ishikawa, *"Flow of a circulating tumor cell and red blood cells in microvessels,"* Phys. Rev. E **92**, 063011 (2015).
[368] W. Wang, T. G. Diacovo, J. Chen, J. B. Freund, and M. R. King, *"Simulation of Platelet, Thrombus and Erythrocyte Hydrodynamic Interactions in a 3D Arteriole with In Vivo Comparison,"* PLoS ONE **8**, e76949 (2013).
[369] J. B. Freund and J. Vermot, *"The Wall-stress Footprint of Blood Cells Flowing in Microvessels,"* Biophys. J. **106**, 752 (2014).
[370] A. Bransky, N. Korin, Y. Nemirovski, and U. Dinnar, *"Correlation between erythrocytes deformability and size: A study using a microchannel based cell analyzer,"* Microvasc. Res. **73**, 7 (2007).
[371] R. S. Franco, M. E. Puchulu-Campanella, L. A. Barber, M. B. Palascak, C. H. Joiner, P. S. Low, and R. M. Cohen, *"Changes in the properties of normal human red blood cells during in vivo aging,"* Am. J. Hematol. **88**, 44 (2013).
[372] R. Malka, F. F. Delgado, S. R. Manalis, and J. M. Higgins, *"In Vivo Volume and Hemoglobin Dynamics of Human Red Blood Cells,"* PLOS Comput. Biol. **10**, e1003839 (2014).
[373] S. Weinbaum, J. M. Tarbell, and E. R. Damiano, *"The Structure and Function of the Endothelial Glycocalyx Layer,"* Annu. Rev. Biomed. Eng. **9**, 121 (2007).
[374] C. S. Alphonsus and R. N. Rodseth, *"The endothelial glycocalyx: A review of the vascular barrier,"* Anaesthesia **69**, 777 (2014).
[375] D. J. Steigmann and R. W. Ogden, *"Elastic surface—substrate interactions,"* Proc. R. Soc. Lond. Math. Phys. Eng. Sci. **455**, 437 (1999).
[376] J. C. Simo and D. D. Fox, *"On a stress resultant geometrically exact shell model. Part I: Formulation and optimal parametrization,"* Comput. Methods Appl. Mech. Eng. **72**, 267 (1989).
[377] W. H. Press, S. A. Teukolsky, W. T. Vetterling, and B. P. Flannery, *Numerical Recipes 3rd Edition: The Art of Scientific Computing*, 3rd ed. (Cambridge University Press, New York, 2007).
[378] E. Evans and Y.-C. Fung, *"Improved measurements of the erythrocyte geometry,"* Microvasc. Res. **4**, 335 (1972).

Appendix A: Derivation of the Euler-Lagrange equation via thin shell theory

While abundant literature on the derivation of the Euler-Lagrange equation (7) via the variational principle is available [24, 36, 41, 57–61, 63, 64, 66, 75], completely worked out derivations by means of the Kirchhoff-Love thin shell theory are much harder to find. This theory is based upon the assumptions that deformations do not change the thickness and that normals to the mid-surface remain normal after deformation [78, 111]. Here we provide such a full derivation, with two major purposes in mind: First, to demonstrate clearly and in a consistent framework the equivalence of the variational and the thin shell approach. Second, to obtain the precise relationship between the often used linear bending models mentioned in sec. II A 2 b and the Helfrich model. We show that these linear bending models lead to a traction jump whose leading order term is equivalent to the leading order term from the full Helfrich equation (7). Higher order terms usually differ. To this end, it will not suffice to use equations that only hold for small deformations as employed e.g. by Pozrikidis [35, p. 272] [54, p. 277]. Steigmann [76] and Naghdi [78] provide an appropriate formalism for finite deformations which we are going to adopt in the present work. Also see Sauer and Duong for a concise overview [112].

1. Differential geometry

We will use the formalism of differential geometry to describe the surface. A very good introduction can be found in the recent review by Deserno [36], and we will only summarize the required notations and results below.

As a start, we introduce two curvilinear coordinates θ^1 and θ^2 and the chart $\boldsymbol{x}(\theta^1, \theta^2)$ that describes the deformed surface.[5] The (in general non-unit) tangent vectors are given by [36, eq. (4)]

$$\boldsymbol{a}_\alpha := \boldsymbol{x}_{,\alpha} \equiv \frac{\partial \boldsymbol{x}}{\partial \theta^\alpha}\,, \tag{A1}$$

where Greek indices assume the values 1 and 2, and the comma denotes the partial derivative with respect to θ^α acting on each Cartesian component. We further introduce the normalized normal vector

$$\boldsymbol{n} := \frac{\boldsymbol{a}_1 \times \boldsymbol{a}_2}{|\boldsymbol{a}_1 \times \boldsymbol{a}_2|}\,, \tag{A2}$$

the symmetric metric tensor (coefficients of the first fundamental form) [36, eq. (8)]

$$a_{\alpha\beta} := \boldsymbol{a}_\alpha \cdot \boldsymbol{a}_\beta\,, \tag{A3}$$

its determinant [36, eq. (13)]

$$a := \det a_{\alpha\beta} = a_{11}a_{22} - a_{12}a_{21} \tag{A4}$$

and the symmetric curvature tensor (coefficients of the second fundamental form) [36, eq. (15)]

$$b_{\alpha\beta} := -\boldsymbol{a}_{\alpha,\beta} \cdot \boldsymbol{n} = \boldsymbol{a}_\alpha \cdot \boldsymbol{n}_{,\beta}\,. \tag{A5}$$

Note that here we use the convention of Deserno regarding the sign, meaning that the mean curvature of a sphere will be positive. Steigmann [76] uses the opposite sign.

The mean curvature is given by [76, eq. (3.8)] [78, eq. (A.2.28)]

$$H := \frac{1}{2}\operatorname{trace}(b^\alpha_\beta) = \frac{1}{2}b^\alpha_\alpha = \frac{1}{2}a^{\alpha\beta}b_{\alpha\beta}\,, \tag{A6}$$

and the Gaussian curvature by [76, eq. (3.8)] [78, eq. (A.2.29)]

$$K := \det b^\alpha_\beta = b^1_1 b^2_2 - b^1_2 b^2_1 = \frac{1}{2}\hat{\varepsilon}^{\alpha\beta}\hat{\varepsilon}^{\lambda\mu}b_{\alpha\lambda}b_{\beta\mu}\,. \tag{A7}$$

Here, $\hat{\varepsilon}^{\alpha\beta} := e^{\alpha\beta}/\sqrt{a}$, with the antisymmetric tensor $e^{\alpha\beta}$ defined by $e^{11} = e^{22} = 0$, $e^{12} = 1$ and $e^{21} = -1$. Summation over repeated indices is implied.

We will need a few more results from differential geometry. To this end, we first introduce the tensor [76, eq. (6.7)]

$$\tilde{b}^{\alpha\beta} := 2Ha^{\alpha\beta} - b^{\alpha\beta}\,. \tag{A8}$$

With this, we summarize the following relations:

$$\boldsymbol{n}_{;\alpha} = b^\beta_\alpha \boldsymbol{a}_\beta\,, \quad \text{(Weingarten) [36, eq. (37a)]} \tag{A9a}$$
$$\boldsymbol{a}_{\alpha;\beta} = -b_{\alpha\beta}\boldsymbol{n}\,, \quad \text{(Gauss) [36, eq. (37b)]} \tag{A9b}$$
$$a^{\alpha\beta}_{;\gamma} = 0\,, \quad \text{[36, eq. (27)]} \tag{A9c}$$
$$\tilde{b}^{\alpha\beta}_{;\alpha} = 0\,, \quad \text{[76, eq. (6.6)]} \tag{A9d}$$
$$a^{\alpha\beta}b_{\alpha\beta} = 2H\,, \quad \text{[36, eq. (17)]} \tag{A9e}$$
$$b^\alpha_\mu \tilde{b}^{\mu\beta} = Ka^{\alpha\beta}\,, \quad \text{[76, eq. (6.14)]} \tag{A9f}$$
$$\phi_{;\alpha} = \phi_{,\alpha}\,, \quad \text{[36, below eq. (26)]} \tag{A9g}$$
$$\phi_{;\beta;\alpha}a^{\alpha\beta} = \Delta_S\phi\,, \quad \text{[36, eq. (32)]} \tag{A9h}$$

where ϕ is some scalar valued function and Δ_S the Laplace-Beltrami operator. The semicolon denotes the *covariant* derivative defined with respect to $a^{\alpha\beta}$ [36, eq. (24a)]. Note that covariant derivatives do not commute in general [36, eq. (34)], and that eq. (A9g) does not hold if ϕ is a tensor density with non-zero weight such as a [36, footnote 9]. Another relation that will be needed is

$$\tilde{b}^{\alpha\gamma}b_{\gamma\beta} = a_{\beta\lambda}b^\lambda_\gamma\tilde{b}^{\alpha\gamma} = Ka_{\beta\lambda}a^{\lambda\alpha} = K\delta^\alpha_\beta\,, \tag{A10}$$

where the usual rising operation [36, eq. (10)] was used for the first equal sign, then eq. (A9f), and finally the Kronecker-delta δ^α_γ [36, eq. (9)]. Also remember that the

[5] In general, several charts will be required [36].

metric and curvature tensors are symmetric. This leads to

$$\tilde{b}^{\alpha\beta}b_{\alpha\beta} = K\delta^\alpha_\alpha = 2K\,. \tag{A11}$$

Combination with eq. (A8) gives [58, eq. (2.34)]

$$b^{\alpha\gamma}b_{\gamma\beta} = 2Hb^\alpha_\beta - K\delta^\alpha_\beta \tag{A12}$$

and

$$b^{\alpha\beta}b_{\alpha\beta} = 4H^2 - 2K\,. \tag{A13}$$

Moreover, using eqs. (A8), (A9c), (A9d) and (A9g) we can also derive

$$b^{\alpha\beta}_{;\alpha} = 2H_{,\alpha}a^{\alpha\beta}\,. \tag{A14}$$

2. Thin shell theory

Performing a force balance for a small patch of the surface [35, 111], one can derive the local equilibrium balance from equation (5) as [76, eq. (2.1)] [78, eq. (9.13)]

$$\boldsymbol{T}^\alpha_{;\alpha} + \triangle\boldsymbol{f}_\mathrm{B} = 0\,. \tag{A15}$$

$\triangle\boldsymbol{f}_\mathrm{B}$ is the traction jump due to the flows (as in eq. (5)) and $\boldsymbol{T}^\alpha$ are two stress vectors.[6] If inertia plays a role, an additional term would need to be taken into account [78, 111, 112]. For simplicity we will restrict ourselves to the interior of the surfaces, i.e. we will not consider the boundaries of open objects.

To continue, we separate $\boldsymbol{T}^\alpha$ into tangential and normal components:

$$\boldsymbol{T}^\alpha = \boldsymbol{N}^\alpha + S^\alpha\boldsymbol{n}\,, \tag{A16}$$

with [76, eq. (2.4)]

$$\boldsymbol{N}^\alpha := N^{\beta\alpha}\boldsymbol{a}_\beta\,, \tag{A17}$$

where $N^{\alpha\beta}$ is an in-plane tension tensor and S^α represents the transverse shear tension [35]. Note that $N^{\alpha\beta}$ is in general not symmetric [112]. Furthermore, we introduce a tension tensor $\sigma^{\alpha\beta}$ via [76, eq. (2.5)]

$$N^{\alpha\beta} = \sigma^{\alpha\beta} + b^\alpha_\mu M^{\mu\beta}\,, \tag{A18}$$

where $M^{\alpha\beta}$ are bending moments [35]. Finally, we have from a local torque balance[7] [76, eq. (2.9)] [35, ch. 4.2]

$$S^\alpha = -M^{\alpha\beta}_{;\beta}\,. \tag{A19}$$

$\sigma^{\alpha\beta}$ (or equivalently $N^{\alpha\beta}$) and $M^{\alpha\beta}$ are determined from appropriate constitutive laws. One possibility is to specify them directly [54, 58, 79–81, 83–85]. Alternatively, they may be derived from a postulated energy density function. To this end, we introduce the energy per unit undeformed area ε. Assuming a homogeneous mass density, $\sigma^{\alpha\beta}$ and $M^{\alpha\beta}$ are then determined by

$$\sigma^{\alpha\beta} = \frac{1}{J}\left(\frac{\partial\varepsilon}{\partial a_{\alpha\beta}} + \frac{\partial\varepsilon}{\partial a_{\beta\alpha}}\right)\,, \tag{A20a}$$

$$M^{\alpha\beta} = \frac{1}{2J}\left(\frac{\partial\varepsilon}{\partial b_{\alpha\beta}} + \frac{\partial\varepsilon}{\partial b_{\beta\alpha}}\right) \tag{A20b}$$

(compare [77, eq. (25)] [76, eq. (2.6)], [111, eq. (4.9)] and [78, eq. (15.15)] with the help of footnote 7). Note that for example $\left(\frac{\partial\epsilon}{\partial a_{\alpha\beta}} + \frac{\partial\epsilon}{\partial a_{\beta\alpha}}\right)/2$ is sometimes simply written as $\frac{\partial\epsilon}{\partial a_{\alpha\beta}}$ [78, p. 537] [375, eq. (3.16)]. The local area dilation is given by [76, eq. (2.7)] [77]

$$J := \sqrt{a/A}\,. \tag{A21}$$

Here, A is the determinant of the metric tensor of the reference surface.

To be more precise, the energy density ε only determines the *symmetric* parts of $\sigma^{\alpha\beta}$ and $M^{\alpha\beta}$ because the right-hand side in eq. (A20) only contains symmetric expressions. The skew (or antisymmetric) parts are undetermined at first [78, p. 537 and p. 551]. However, the skew part of the bending moments $M^{\alpha\beta}$ plays no role in this case and can be set to zero [78, eq. (15.17)] without loss of generality [111, p. 285], making $M^{\alpha\beta}$ symmetric. Moreover, a local torque balance can be used to derive (compare [112] [78, eq. (10.21)] [111, eq. (6.1)] [35, eq. (4.14)] [84, eq. (22b)] [58, eq. (A.8)] while keeping footnote 7 in mind)

$$e_{\alpha\beta}(N^{\alpha\beta} - b^\alpha_\mu M^{\mu\beta}) = 0\,. \tag{A22}$$

The antisymmetric tensor $e_{\alpha\beta}$ has been introduced above. This equation fixes the skew part of $N^{\alpha\beta}$ [78, eq. (15.18)]

[6] Deserno [36] calls $-\boldsymbol{T}^\alpha$ the surface stress tensor and denotes it by "$\boldsymbol{f}^a$".

[7] Note that for most of the quantities different conventions exist; here we follow reference [76]. Most importantly, $N^{\alpha\beta}$ from eq. (A17) might be defined transposed as $\boldsymbol{N}^\alpha = N^{\alpha\beta}\boldsymbol{a}_\beta$ [78, eq. (9.40)], and $M^{\alpha\beta}$ might be obtained from a derivative with respect to $-b_{\alpha\beta}$ in eq. (A20b) [78, eq. (5.61),(15.15)] [111, eq. (4.9)]. If only the $-b_{\alpha\beta}$ derivative convention is used, eq. (A18) becomes $N^{\alpha\beta} = \sigma^{\alpha\beta} - b^\alpha_\mu M^{\mu\beta}$ [111, eq. (4.9)] and eq. (A19) becomes $S^\alpha = M^{\alpha\beta}_{;\beta}$ [111, eq. (5.3)] [84, eq. (22a)] [58, eq. (A.7)] [35, eq. (4.14)]. If additionally the transposed convention is employed, we have $N^{\alpha\beta} = \sigma^{\alpha\beta} - b^\beta_\mu M^{\mu\alpha}$ [78, eq. (10.26)]. Naturally, these two conventions also change eq. (A22). We also remark that the sign convention for the curvature tensor (A5) is independent of this.

by implying that the skew part of $\sigma^{\alpha\beta}$ should be zero, i.e. that $\sigma^{\alpha\beta}$ must be symmetric [112, eq. (71)]. Thus, in short, one can take eqs. (A20) to define $\sigma^{\alpha\beta}$ and $M^{\alpha\beta}$ completely, and eq. (A22) will be satisfied automatically [111].[8]

Before we continue, we derive explicit expressions for the tangential (f^β) and normal (f^3) components of the traction jump

$$\triangle \boldsymbol{f}_\mathrm{B} = f^\beta \boldsymbol{a}_\beta + f^3 \boldsymbol{n} \,. \tag{A23}$$

To this end, rewrite

$$\begin{aligned}\boldsymbol{T}^\alpha_{;\alpha} &= (N^{\beta\alpha}\boldsymbol{a}_\beta)_{;\alpha} + (S^\alpha \boldsymbol{n})_{;\alpha} \\ &= N^{\beta\alpha}_{;\alpha}\boldsymbol{a}_\beta + N^{\beta\alpha}\boldsymbol{a}_{\beta;\alpha} + S^\alpha_{;\alpha}\boldsymbol{n} + S^\alpha \boldsymbol{n}_{;\alpha} \,.\end{aligned}$$

Using eqs. (A9a) and (A9b), we find

$$\boldsymbol{T}^\alpha_{;\alpha} = (S^\alpha b^\beta_\alpha + N^{\beta\alpha}_{;\alpha})\boldsymbol{a}_\beta + (S^\alpha_{;\alpha} - N^{\beta\alpha}b_{\beta\alpha})\boldsymbol{n} \,. \tag{A24}$$

Hence, eq. (A15) can be written as

$$f^\beta = -S^\alpha b^\beta_\alpha - N^{\beta\alpha}_{;\alpha} \,, \tag{A25a}$$

$$f^3 = -S^\alpha_{;\alpha} + N^{\alpha\beta}b_{\alpha\beta} \,. \tag{A25b}$$

These equations match with references [76, eq. (6.17)] (mind the H sign convention), [78, eq. (15.20)] [58, eq. (A9),(A10)] (mind footnote 7) as well as with [84, eq. (23)] [86, eq. (A18),(A19)] [35, eq. (4.13)] (mind footnote 7 and the H sign).

Given an energy density ε, equations (A15) – (A20) fully determine the traction jump $\triangle \boldsymbol{f}_\mathrm{B}$. Hence, the goal will be to apply this formalism to the Helfrich model from equation (1). To this end, note again that ε is the energy per unit *undeformed* area [77], i.e. the total energy of some surface patch is given by $\int \varepsilon \,\mathrm{d}S_0$ where the integration goes over the undeformed surface (compare [111, eq. (2.19)] and refs. [43, 77]). The Helfrich energy density ϵ_B as in the main text, however, is usually specified per unit *deformed* area, i.e. the total energy is $\int \epsilon_\mathrm{B} \,\mathrm{d}S$. Considering that $\mathrm{d}S_0 = \sqrt{A}\,\mathrm{d}\theta^1\mathrm{d}\theta^2$ and $\mathrm{d}S = \sqrt{a}\,\mathrm{d}\theta^1\mathrm{d}\theta^2$ [36, eq. (84)], and furthermore demanding that $\varepsilon \,\mathrm{d}S_0 \overset{!}{=} \epsilon_\mathrm{B}\,\mathrm{d}S$, we find with equation (A21) [77]

$$\varepsilon = J\,\epsilon_\mathrm{B} \,. \tag{A26}$$

Thus, for the Helfrich model from eq. (1) [76, eq. (7.17)]:

$$\varepsilon = J\,\left[2\kappa_\mathrm{B}(H-H_0)^2 + \kappa_\mathrm{K}K\right] \,. \tag{A27}$$

3. Derivation of the traction jump for a general energy functional

a. *Intermediary results*

To start the derivation of general formulas, we use that the bending contribution to ε for fluid membranes can only depend on J, H and K [43]:

$$\varepsilon = \varepsilon(J,H,K) \,. \tag{A28}$$

The Helfrich model is contained as a special case. Using the chain rule, we find for eqs. (A20) [76, eq. (6.13)]

$$\begin{aligned}\sigma^{\alpha\beta} &= -\frac{1}{J}\left(-J\varepsilon_{,J} + 2K\varepsilon_{,K} + 2H\varepsilon_{,H}\right)a^{\alpha\beta} \\ &\quad + \varepsilon_{,H}\tilde{b}^{\alpha\beta}/J \,,\end{aligned} \tag{A29a}$$

$$M^{\alpha\beta} = -\frac{1}{J}\left(\frac{1}{2}\varepsilon_{,H}a^{\alpha\beta} + \varepsilon_{,K}\tilde{b}^{\alpha\beta}\right) \,, \tag{A29b}$$

where $\tilde{b}^{\alpha\beta}$ was defined in equation (A8). Furthermore, using eqs. (A9c) and (A9d), we obtain for the transverse shear tension in eq. (A19) [76, eq. (6.18)]

$$S^\alpha = \frac{1}{2}\left(\varepsilon_{,H}/J\right)_{;\beta}a^{\alpha\beta} + \left(\varepsilon_{,K}/J\right)_{;\beta}\tilde{b}^{\alpha\beta} \,. \tag{A30}$$

The next step is to compute $N^{\alpha\beta}$ from equation (A18). In order to facilitate the connection with the linear bending models later on, we separate the contributions by introducing two *artificial* parameters ζ and ξ:

$$N^{\alpha\beta} = \zeta\sigma^{\alpha\beta} + \xi b^\alpha_\mu M^{\mu\beta} \,. \tag{A31}$$

Setting $\zeta = \xi = 1$ recovers the full equations. Next, compute

$$b^\alpha_\mu M^{\mu\beta} = \frac{1}{2J}\varepsilon_{,H}b^{\alpha\beta} + \frac{\varepsilon_{,K}}{J}Ka^{\alpha\beta} \,, \tag{A32}$$

where eq. (A9f) and the usual rising operations [36, eq. (10)] have been used. Using the definition of $\tilde{b}^{\alpha\beta}$, equation (A31) assumes the form

$$\begin{aligned}N^{\alpha\beta} = &-\frac{1}{J}\left[-J\zeta\varepsilon_{,J} + (2\zeta-\xi)K\varepsilon_{,K}\right]a^{\alpha\beta} \\ &-\frac{1}{2J}(2\zeta-\xi)\varepsilon_{,H}b^{\alpha\beta} \,.\end{aligned} \tag{A33}$$

b. *Tangential component*

The tangential components of the traction jump are given via equation (A25a). Using eqs. (A9c), (A9f) and (A14), we find

$$\begin{aligned}f^\beta = &\frac{1}{2}(2\zeta-\xi-1)(\varepsilon_{,H}/J)_{;\alpha}b^{\alpha\beta} \\ &+\Big[\left(-\zeta\varepsilon_{,J} + (2\zeta-\xi)K\varepsilon_{,K}/J\right)_{;\alpha} \\ &\quad -(\varepsilon_{,K}/J)_{;\alpha}K \\ &\quad +(2\zeta-\xi)H_{,\alpha}\varepsilon_{,H}/J\Big]a^{\alpha\beta} \,,\end{aligned} \tag{A34}$$

or for the true values $\xi = \zeta = 1$

$$\begin{aligned}f^\beta = &\Big[\left(-\varepsilon_{,J} + K\varepsilon_{,K}/J\right)_{;\alpha} - (\varepsilon_{,K}/J)_{;\alpha}K \\ &+H_{,\alpha}\varepsilon_{,H}/J\Big]a^{\alpha\beta} \,.\end{aligned} \tag{A35}$$

[8] Note, that if some constitutive laws for $N^{\alpha\beta}$ and $M^{\alpha\beta}$ are provided directly rather than via some energy density (as is done for some of the linear bending models of section A 5), eq. (A22) constitutes a restriction for the possible laws [376, ch. 4].

c. Normal component

To evaluate eq. (A25b), first calculate

$$S^{\alpha}_{;\alpha} = \frac{1}{2}\Delta_{\mathrm{S}}\left(\varepsilon_{,H}/J\right) + \left(\varepsilon_{,K}/J\right)_{;\alpha;\beta}\tilde{b}^{\alpha\beta}\,, \tag{A36}$$

where we used eqs. (A9c), (A9d), (A9g) and (A9h) and the symmetry of $\tilde{b}^{\alpha\beta}$ to exchange the covariant derivatives. Using eqs. (A9e), (A8) and (A13), we obtain the general result for arbitrary ζ, ξ and $\varepsilon(J,H,K)$

$$\begin{aligned} f^3 = &-\frac{1}{2}\Delta_{\mathrm{S}}(\varepsilon_{,H}/J) - (\varepsilon_{,K}/J)_{;\alpha;\beta}\tilde{b}^{\alpha\beta} \\ &- \frac{2H}{J}\left[-\zeta J\varepsilon_{,J} + (2\zeta-\xi)K\varepsilon_{,K}\right] \\ &- \frac{2\zeta-\xi}{J}(2H^2-K)\varepsilon_{,H}\,, \end{aligned} \tag{A37}$$

or for the true values $\xi = \zeta = 1$

$$\begin{aligned} f^3 = &-\frac{1}{2}\Delta_{\mathrm{S}}(\varepsilon_{,H}/J) - (\varepsilon_{,K}/J)_{;\alpha;\beta}\tilde{b}^{\alpha\beta} \\ &- \frac{2H}{J}\left[-J\varepsilon_{,J} + K\varepsilon_{,K}\right] \\ &- \frac{1}{J}(2H^2-K)\varepsilon_{,H}\,. \end{aligned} \tag{A38}$$

This is the final general formula for the normal component of the traction jump.

4. Derivation of the traction jump for the Helfrich model

We will now specialize the above relations for the Helfrich model from eq. (A27) for constant κ_{B} and κ_{K}. For convenient comparison with the literature, we will also provide intermediary results.

a. Intermediary results

First of all, from eqs. (A29) we find the symmetric tension tensor $\sigma^{\alpha\beta}$ and the bending moments as [77, eq. (28)]

$$\begin{aligned} \sigma^{\alpha\beta} &= \left[2\kappa_{\mathrm{B}}(H-H_0)^2 - \kappa_{\mathrm{K}}K\right]a^{\alpha\beta} \\ &\quad - 4\kappa_{\mathrm{B}}(H-H_0)b^{\alpha\beta}\,, && \text{(A39a)} \\ M^{\alpha\beta} &= -2\kappa_{\mathrm{B}}(H-H_0)a^{\alpha\beta} - \kappa_{\mathrm{K}}\tilde{b}^{\alpha\beta}\,. && \text{(A39b)} \end{aligned}$$

Hence, the transverse shear tension (A30) is given by

$$S^{\alpha} = 2\kappa_{\mathrm{B}}(H-H_0)_{;\beta}\,a^{\alpha\beta}\,, \tag{A40}$$

and the full in-plane tension tensor (A33) is

$$\begin{aligned} N^{\alpha\beta} = &\left[2\kappa_{\mathrm{B}}\zeta(H-H_0)^2 - (\zeta-\xi)\kappa_{\mathrm{K}}K\right]a^{\alpha\beta} \\ &- 2\kappa_{\mathrm{B}}(2\zeta-\xi)(H-H_0)b^{\alpha\beta}\,. \end{aligned} \tag{A41}$$

Also note that for $\xi = \zeta = 1$ (the correct values), one directly finds [77, eq. (28)]

$$N^{\alpha\beta} = 2\kappa_{\mathrm{B}}(H-H_0)^2a^{\alpha\beta} - 2\kappa_{\mathrm{B}}(H-H_0)b^{\alpha\beta}\,, \tag{A42}$$

i.e. the result is independent of the saddle-splay modulus κ_{K}.

We shortly stop at this point and actually compute the stress vectors $\boldsymbol{T}^{\alpha}$ from equation (A16). A short computation shows for $\zeta = \xi = 1$:

$$\begin{aligned} \boldsymbol{T}^{\alpha} = &2\kappa_{\mathrm{B}}(H-H_0)^2a^{\alpha\beta}\boldsymbol{a}_{\beta} \\ &- 2\kappa_{\mathrm{B}}(H-H_0)b^{\alpha\beta}\boldsymbol{a}_{\beta} \\ &+ 2\kappa_{\mathrm{B}}(H-H_0)_{,\beta}a^{\alpha\beta}\boldsymbol{n}\,. \end{aligned} \tag{A43}$$

This expression for the stress vectors matches with the surface stress tensor from ref. [36, eq. (96)] for a constant H_0 and refs. [61, eq. (51)] [62, eq. (14)] for $H_0 = 0$ up to a definition-implied global sign. It also agrees with references [70, eq. (2.64)] and [57, eq. (128)]. As explained in ref. [36], $\boldsymbol{T}^{\alpha}$ represent a first integral of the Euler-Lagrange equation.

b. Tangential component

Substituting eq. (A27) into eq. (A34) gives the following tangential components of the traction jump:

$$\begin{aligned} f^{\beta} = &2\kappa_{\mathrm{B}}(2\zeta-\xi-1)(H-H_0)_{,\alpha}b^{\alpha\beta} \\ &+ \left[4\kappa_{\mathrm{B}}(H-H_0)H_{,\alpha} + \kappa_{\mathrm{K}}K_{,\alpha}\right](\zeta-\xi)a^{\alpha\beta}\,. \end{aligned} \tag{A44}$$

For $\zeta = \xi = 1$ this obviously reduces to

$$f^{\beta} = 0\,. \tag{A45}$$

Thus, for the actual Helfrich model the tangential tractions vanish in the interior of the surface if no additional constraints are used.

c. Normal component

It is straightforward to evaluate eq. (A37) with ε from eq. (A27). The result is

$$\begin{aligned} f^3 = &-2\kappa_{\mathrm{B}}\Big\{\Delta_{\mathrm{S}}(H-H_0) \\ &+ 2(H-H_0)\Big[(2\zeta-\xi)(2H^2-K) \\ &\qquad - \zeta H(H-H_0)\Big]\Big\} \\ &- 2\kappa_{\mathrm{K}}(\zeta-\xi)HK\,, \end{aligned} \tag{A46}$$

or for $\xi = \zeta = 1$

$$\begin{aligned} f^3 = &-2\kappa_{\mathrm{B}}[\Delta_{\mathrm{S}}(H-H_0) \\ &+ 2(H-H_0)(H^2-K+H_0H)]\,. \end{aligned} \tag{A47}$$

Taking eq. (A23) into account, the results (A45) and (A47) match *exactly* with the one from eq. (7) obtained via a variational derivative. Thus, the variational and the shell theory approaches are compatible with each other and lead to the same results. Also note that the κ_K term drops out, as required by the Gauss-Bonnet theorem. We further remark that the Laplace-Beltrami term in eq. (A46) is always there, regardless of the values of κ_K, ξ and ζ.

d. *Order of the individual terms*

In view of the linear bending models presented in the next section, it is of some interest to know the importance of the individual terms occurring in equation (A47). To this end, consider a general surface in the Monge gauge [36]: At least locally, the surface can be described by the vector $\widetilde{\boldsymbol{x}}(x,y) := (x,y,h(x,y)) \in \mathbb{R}^3$ with the height function h. We assume that the deviations from a plane are of order $\psi > 0$, i.e. $h_{,x} \sim \mathcal{O}(\psi)$ and $h_{,y} \sim \mathcal{O}(\psi)$. Next, a deformation $\boldsymbol{u} \in \mathbb{R}^3$ leads to the deformed surface $\boldsymbol{x}(x,y) := \widetilde{\boldsymbol{x}}(x,y) + \boldsymbol{u}(x,y)$. The deformation shall be of order $\chi > 0$, i.e. $\boldsymbol{u}_{,x} \sim \mathcal{O}(\chi)$ and $\boldsymbol{u}_{,y} \sim \mathcal{O}(\chi)$. Furthermore, we set the reference shape (but not the undeformed state $\widetilde{\boldsymbol{x}}$) to be a flat plane ($H_0 = 0$).

With this we can compute the various geometric quantities for the deformed surface $\boldsymbol{x}$ to leading orders, similar to reference [86]. In the end, we obtain

$$\Delta_\mathrm{S} H \sim \mathcal{O}(\psi) + \mathcal{O}(\chi) + \mathcal{O}(\psi\chi) + \text{h.o.}\,, \tag{A48a}$$

$$H(H^2 - K) \sim \mathcal{O}(\chi\psi^2) + \text{h.o.}\,, \tag{A48b}$$

and for the full normal component

$$f^3 \boldsymbol{n} \sim \mathcal{O}(\psi) + \mathcal{O}(\chi) + \mathcal{O}(\psi\chi) + \text{h.o.}\,, \tag{A48c}$$

where "h.o." stands for "higher orders". Hence, at least for small deviations from a plane ($\psi, \chi \ll 1$) we have $|\Delta_\mathrm{S} H| \gg |H(H^2 - K)|$, which is consistent with reference [86, eq. (A20)].

This also seems to hold for larger deviations from a plane. For example, for the typical RBC shape from equation (B14) and figure 2, $\Delta_\mathrm{S} H$ is found to be up to almost one order of magnitude larger than the others, i.e. [27]

$$\max|2\Delta_\mathrm{S} H| \approx 218\,, \tag{A49a}$$

$$\max|4H(H^2 - K)| \approx 28.8\,, \tag{A49b}$$

$$\max|f^3 \boldsymbol{n}| \approx 189 \tag{A49c}$$

(units chosen such, that the large RBC radius is 1 and $\kappa_\mathrm{B} = 1$).

5. Linear bending models

Some authors use a so-called "linear bending model" instead of the Helfrich model as already described in sec. II A 2 b of the main text. The purpose of this section is to shed some light on the relationship between these two types. In linear bending models, the bending moments and in-plane tensions are not derived from an energy functional as in eqs. (A20a) and (A20b). Instead, their form is given by postulated constitutive laws. A common assumption of such models is that the saddle splay modulus κ_K plays no role (which is always true for closed objects with constant topology).

In the following we will consider four such models (a – d) which are similar, but not identical.

a. Model a The first constitutive law we consider is the "linear isotropic model" presented e.g. by Pozrikidis [80, eq. (10)] [81, eq. (2.5.11)]

$$M^{\alpha\beta} = -2\kappa_\mathrm{B}(H - H_0)a^{\alpha\beta}\,. \tag{A50}$$

It is further *assumed* [54, p. 277] that only the *antisymmetric* components of the in-plane tension tensor $N^{\alpha\beta}$ are affected by the bending rigidity, namely via eq. (A22). Due to the particular form of $M^{\alpha\beta}$, this contribution however amounts to zero, i.e. we have in total

$$N^{\alpha\beta} = 0\,. \tag{A51}$$

Note that additional material properties (such as resistance against shearing) might still lead to a non-zero total $N^{\alpha\beta}$. The two equations (A50) and (A51) are captured by $\kappa_\mathrm{K} = 0$ and $\zeta = \eta = 0$ in our general framework presented above (cf. eqs. (A31) and (A39b)). The resulting traction jump is therefore obtained via eqs. (A46) and (A44) as

$$f^\beta = -2\kappa_\mathrm{B}(H - H_0)_{,\alpha} b^{\alpha\beta}\,, \tag{A52a}$$

$$f^3 = -2\kappa_\mathrm{B}\Delta_\mathrm{S}(H - H_0)\,. \tag{A52b}$$

Considering expression (A48), the normal component matches to leading orders with the result (A47) for the Helfrich model. Interestingly, an additional tangential component arises. For the series expansion similar to eq. (A48) we find $f^\beta \boldsymbol{a}_\beta \sim \mathcal{O}(\psi\chi) + \text{h.o.}$, and so the normal component dominates at least for $\psi, \chi \ll 1$. This is affirmed for the typical RBC shape, where $\max|f^\beta \boldsymbol{a}_\beta| \approx 62.7$ which is less than one third of the value for the normal component (A52b) (see eq. (A49a)). Moreover, figure 6 depicts the complete traction jumps and the relative deviation to the Helfrich model for the RBC shape. In the rather flat dimple regions, the deviations are small ($\lesssim 5\,\%$) which is in agreement with the series expansion; they only become larger in the high curvature regime. Thus, all in all, the complete traction jump $\triangle \boldsymbol{f}_\mathrm{B}$ of model a matches with the Helfrich model to leading order $\mathcal{O}(\psi) + \mathcal{O}(\chi)$.

b. Model b Another model that has sometimes been used [80, eq. (8)] [81, eq. (2.5.9)] [83, eq. (25)] [54, eq. (4.6)] [5, eq. (23)] is given by

$$M^{\alpha\beta} = -\kappa_\mathrm{B}(b^{\alpha\beta} - 2H_0 a^{\alpha\beta})\,. \tag{A53}$$

$N^{\alpha\beta}$ is once again determined via eq. (A22) (assumption of no symmetric components), and once again the skew

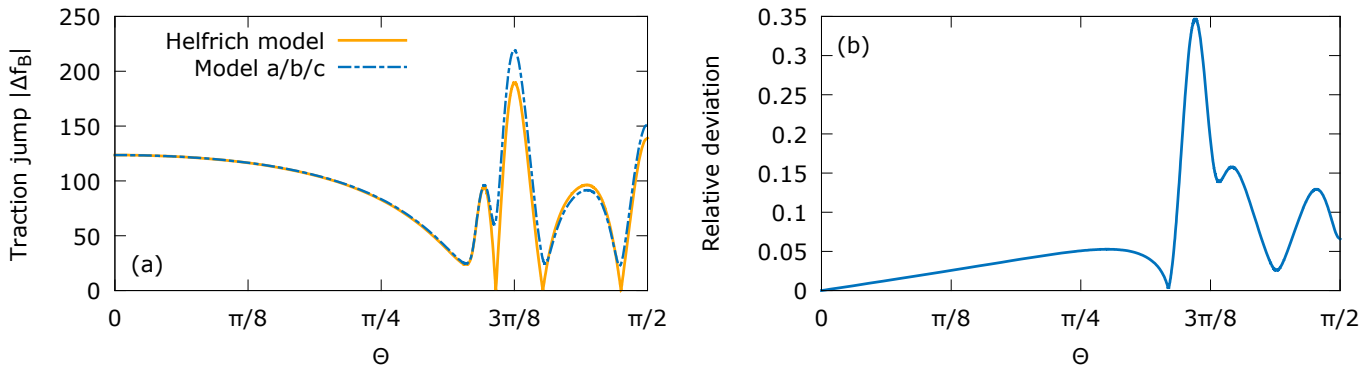

Figure 6. Comparison between the traction jumps of the Helfrich model and the linear bending models for the typical red blood cell shape from figure 2. The spontaneous curvature is set to zero ($H_0 = 0$), in which case linear bending models a, b and c are equivalent. Analytic computations via equation (B14), and the polar angle is defined as $\Theta := \arccos\left(x_3/\sqrt{x_1^2 + x_2^2 + x_3^2}\right)$ with the Cartesian coordinates x_1, x_2 and x_3. Note that the shape is axisymmetric, and thus the results are independent of the azimuthal angle. (a) The magnitude of the full traction jump $|\triangle \boldsymbol{f}_\mathrm{B}|$ (units chosen such, that $\kappa_\mathrm{B} = 1$ and the large RBC radius is 1). (b) Relative deviation $|\triangle \boldsymbol{f}_\mathrm{B}^\mathrm{H} - \triangle \boldsymbol{f}_\mathrm{B}^\mathrm{L}| / \max|\triangle \boldsymbol{f}_\mathrm{B}^\mathrm{H}|$, where the upper indices H and L denote the Helfrich and linear bending models, respectively, and $\max|\triangle \boldsymbol{f}_\mathrm{B}^\mathrm{H}| \approx 189$. Only minor deviations are observed in the rather flat dimple regions ($\Theta \lesssim 5\pi/16$), in agreement with the series expansion from the main text.

part and hence the full $N^{\alpha\beta}$ can be shown to be zero, too. Using eqs. (A19), (A9c) and (A14), we find

$$S^\alpha = 2\kappa_\mathrm{B}(H - H_0)_{,\beta}\, a^{\alpha\beta}\,, \tag{A54}$$

which matches exactly with expression (A40) for the Helfrich model. Considering that $N^{\alpha\beta} = 0$, the traction jump is thus given by eqs. (A46) and (A44) with $\zeta = \eta = 0$:

$$f^\beta = -2\kappa_\mathrm{B}(H - H_0)_{,\alpha} b^{\alpha\beta}\,, \tag{A55a}$$
$$f^3 = -2\kappa_\mathrm{B}\Delta_\mathrm{S}(H - H_0)\,. \tag{A55b}$$

Thus, at least from the viewpoint of the traction jump, models a and b can be considered to be equivalent.

c. Model c Yet another constitutive equation is the one employed by Zhao *et al.* and others [84, eq. (21)] [85, p. 382] [86, eq. (A12)]. Although it is also called "linear isotropic model" in reference [84], its form is slightly different from Pozrikidis's version (eq. (A50)). It is given by

$$M^\alpha_\beta = -\kappa_\mathrm{B}(b^\alpha_\beta - B^\alpha_\beta)\,. \tag{A56}$$

Equation (A22) determines the skew components of $N^{\alpha\beta}$ and the symmetric components of $N^{\alpha\beta}$ are assumed to be independent of the bending rigidity. $B_{\alpha\beta} = -\boldsymbol{X}_{,\alpha\beta} \cdot \boldsymbol{N}$ is the curvature tensor of the reference surface $\boldsymbol{X}(\theta^1, \theta^2)$ (cf. eq. (A5) and [77, eq. (11)]) and $\boldsymbol{N}$ the corresponding normal vector. Furthermore, we have $B^\alpha_\beta = A^{\alpha\gamma}B_{\gamma\beta}$ with the metric tensor $A^{\alpha\beta}$ of the reference state [77]. The in-plane tension tensor is according to eq. (A22) and ref. [78, eq. (15.18)]

$$N^{\alpha\beta} = \frac{1}{2}\kappa_\mathrm{B} B^\mu_\gamma b_{\lambda\mu}(a^{\alpha\lambda}a^{\gamma\beta} - a^{\alpha\gamma}a^{\lambda\beta})\,, \tag{A57}$$

because its symmetric components are assumed to be zero (if no additional elasticities exist). This expression is non-zero for *general* reference states $\boldsymbol{X}$ although some authors assume otherwise [84, 85]. As an example, taking a unit sphere [36, eq. (2b)] for the deformed geometry $\boldsymbol{x}(\theta^1, \theta^2)$ leads to $(N^{\alpha\beta}) = \frac{1}{2}\kappa_\mathrm{B}(B_1^2 - B_2^1/\sin^2\theta^1)\left(\begin{smallmatrix} 0 & -1 \\ 1 & 0 \end{smallmatrix}\right)$ in spherical coordinates, where $\theta^1 \in [0; \pi]$ is the polar angle. Continuing, the components of the traction jump follow from equation (A25) as

$$\begin{aligned} f^\beta = {} & -2\kappa_\mathrm{B} H_{,\alpha} b^{\alpha\beta} + \kappa_\mathrm{B} B^\alpha_{\gamma;\lambda} a^{\gamma\lambda} b^\beta_\alpha \\ & + \tfrac{1}{2}\kappa_\mathrm{B}(B^\mu_\gamma b_{\lambda\mu})_{;\alpha}(a^{\alpha\lambda}a^{\gamma\beta} - a^{\alpha\gamma}a^{\lambda\beta})\,, \end{aligned} \tag{A58a}$$
$$f^3 = -2\kappa_\mathrm{B}\Delta_\mathrm{S} H + \kappa_\mathrm{B} B^\alpha_{\gamma;\beta;\alpha} a^{\gamma\beta}\,. \tag{A58b}$$

The second line for f^β is absent if we assume $N^{\alpha\beta} = 0$. Interestingly, f^3 is always independent of $N^{\alpha\beta}$ for the expression from equation (A57). In any case, the result matches with the previous two models for a flat reference state, but differs for general B^α_β. A precise and concise relationship is unfortunately not easily established. We further remark that application of eq. (A58) to small axisymmetric deformations of a spherical membrane recovers the expressions from reference [309, eq. (A19)] to leading order.

d. Model d Jenkins [58] focuses on the derivation of the Euler-Lagrange equation for the Helfrich model for $H_0 = 0$ via the variational approach. Later on, he postulates some constitutive equations to make the connection between the variational and the thin shell formulation, namely [58, eqs. (A.11), (A.12)]

$$M^{\alpha\beta} = -2\kappa_\mathrm{B} H a^{\alpha\beta}\,, \tag{A59a}$$
$$N^{\alpha\beta} = -2\kappa_\mathrm{B} H b^{\alpha\beta} \tag{A59b}$$

(plus some inextensibility contribution). Most notably there is a non-zero bending contribution to $N^{\alpha\beta}$, contrary to the previous models. He shows that these equations lead to the same Euler-Lagrange equation.

Unfortunately, he made a mistake during his variational derivative. Namely, he forgot to vary the surface element or equivalently $\delta\sqrt{a}$ in [58, eq. (2.18)].[9] This results in $2H^2$ instead of the correct H^2 in the Euler-Lagrange equation (A47). Another consequence is that it leads him to propose an incorrect constitutive law for $N^{\alpha\beta}$. Taking this into account, he would have probably specified the constitutive equations as

$$M^{\alpha\beta} = -2\kappa_\mathrm{B} H a^{\alpha\beta}\,, \tag{A60a}$$
$$N^{\alpha\beta} = 2\kappa_\mathrm{B} H^2 a^{\alpha\beta} - 2\kappa_\mathrm{B} H b^{\alpha\beta}\,. \tag{A60b}$$

Comparing with eqs. (A39b) and (A42), these equations reproduce the traction jump of the Helfrich model (for $H_0 = 0$) exactly.

e. Summary To summarize, the traction jump derived from the linear bending models a and b agree with each other, and with model c at least for zero reference curvatures. Furthermore, all three agree to leading order (i.e. for small deviations from a plane) in the traction jump with the Helfrich law for a flat reference state, where the leading order term is given by $\sim \Delta_\mathrm{S} H$. Perfect agreement with the Helfrich model, however, requires to take into account the non-zero bending contributions to the symmetric part of the in-plane tension tensor $N^{\alpha\beta}$ (model d). These are often neglected, inducing additional tangential components.

6. Inextensibility constraint

Similar to the variational derivative formalism, it is also possible to include the local area incompressibility constraint in the thin-shell derivation. This can be done by adding the term $\int_S \tilde{\sigma}\,\mathrm{d}S$ to the total energy (cf. sec. II A 2 a). This is equivalent to adding $\tilde{\sigma}J$ to eq. (A27), i.e. [76, eq. (2.8)] [112]

$$\varepsilon \to \varepsilon + \tilde{\sigma} J\,, \tag{A61}$$

Here, $\tilde{\sigma} = \tilde{\sigma}(\theta^1, \theta^2)$ is the local Lagrange multiplier. Taking into account that $\tilde{\sigma}$ does not depend on the surface (i.e. neither on J, H or K) but only on the curvilinear coordinates, eq. (A38) then provides the normal contribution

$$f^3 \to f^3 + 2H\tilde{\sigma} \tag{A62}$$

for $\zeta = 1$. On the other hand, the tangential equation (A35) gives

$$f^\beta \to f^\beta - \tilde{\sigma}_{,\alpha} a^{\alpha\beta}\,, \tag{A63}$$

i.e. a non-zero additional term. Using the definition of the surface gradient [52, eq. (60)] given by

$$\boldsymbol{\nabla}_\mathrm{S}\tilde{\sigma} = \tilde{\sigma}_{,\alpha}\boldsymbol{a}^\alpha = \tilde{\sigma}_{,\alpha} a^{\alpha\beta}\boldsymbol{a}_\beta\,, \tag{A64}$$

as well as eq. (A23), the total traction jump thus receives the additional term

$$\triangle \boldsymbol{f}_\mathrm{B} \to \triangle \boldsymbol{f}_\mathrm{B} + 2H\tilde{\sigma}\boldsymbol{n} - \boldsymbol{\nabla}_\mathrm{S}\tilde{\sigma} \tag{A65}$$

due to the inextensibility. Its significance has already been explained in section II A 2 a.

[9] Jenkins additionally integrates over the deformed rather than the undeformed surface for the γ term in [58, eq. (2.18)], leading to an incorrect equation for the surface inextensibility. Otherwise, he would have obtained the correct equation (A65). Nevertheless, this does not affect the bending traction jump itself.

Appendix B: Using spherical harmonics to compute the bending forces

We detail here the direct computation of the traction jump from eq. (7) (strong formulation) using spherical harmonics. The methodology closely follows references [101, 103].

A square-integrable function $f(\vartheta, \varphi)$ with $\vartheta \in [0; \pi]$ and $\varphi \in [0; 2\pi[$ can be expanded into a spherical harmonics series:

$$f(\vartheta, \varphi) = \sum_{l=0}^{\infty} \sum_{m=-l}^{l} \hat{f}_l^m Y_l^m(\vartheta, \varphi)\,. \tag{B1}$$

The coefficients $\hat{f}_l^m \in \mathbb{C}$ are given by an integration over the unit sphere,

$$\hat{f}_l^m = \int_0^\pi \int_0^{2\pi} f(\vartheta, \varphi) \bar{Y}_l^m(\vartheta, \varphi) \sin\vartheta\,\mathrm{d}\varphi\,\mathrm{d}\vartheta\,. \tag{B2}$$

$\bar{Y}_l^m$ is the complex conjugate of the spherical harmonic Y_l^m defined by

$$Y_l^m(\vartheta, \varphi) := \sqrt{\frac{2l+1}{4\pi}\frac{(l-m)!}{(l+m)!}}\,\widetilde{P}_l^m(\vartheta) e^{im\varphi}\,, \tag{B3}$$

with i being the imaginary unit, $\widetilde{P}_l^m(\vartheta) := P_l^m(\cos\vartheta)$ and the associated Legendre polynomials

$$P_l^m(x) := \frac{(-1)^m}{2^l\, l!}(1-x^2)^{m/2}\frac{\mathrm{d}^{l+m}}{\mathrm{d}x^{l+m}}[(x^2-1)^l]\,. \tag{B4}$$

Note that the Condon-Shortley phase $(-1)^m$ is included here. We compute the spherical harmonic Y_l^m via the `C++ boost` library.

Let p be the truncation order for the spherical harmonics expansion. The latitude direction is covered by $p+1$ points $\vartheta_i = \arccos z_i$, $i = 0, \ldots, p$, where z_i are the Gauss-Legendre nodes with corresponding weights ν_i (computable e.g. via the `gauleg` routine from [377]). Integrations are done using the Gauss-Legendre quadrature. Furthermore, we distribute $2p+2$ points equidistantly in the longitudinal direction, i.e. $\varphi_j = \pi j/(p+1)$, $j = 0, \ldots, 2p+1$. Integration in this direction is performed by means of the trapezoidal rule with weights

$\mu_j = \pi/(p+1)$, $j = 0, \dots, 2p+1$ (i.e. every point has the same weight). Hence, equation (B2) is approximated by

$$\hat{f}_l^m \approx \sum_{i=0}^{p} \sum_{j=0}^{2p+1} \nu_i \mu_j f(\vartheta_i, \varphi_j) \bar{Y}_l^m(\vartheta_i, \varphi_j)\,. \tag{B5}$$

These algorithms and integration points are chosen because eq. (B5) is then superalgebraically = exponentially = spectrally convergent with the order p for smooth functions [101]. Note that due to the truncation, we have $l = 0, \dots, p$ and $m = -l, \dots, l$. This also implies

$$f(\vartheta_i, \varphi_j) \approx \sum_{l=0}^{p} \sum_{m=-l}^{l} \hat{f}_l^m Y_l^m(\vartheta_i, \varphi_j)\,. \tag{B6}$$

We remark that the forward and backward transformations can be done using the Fast Fourier Transform (FFT) for the longitude and the Fast Legendre Transform (FLT) for the latitude direction. In practice FLTs are rarely used. For simplicity we also abstain from using FFTs, as they would make the computation of higher order derivatives much more complex.

Derivatives of $f(\vartheta, \varphi)$ can now be rolled off onto the spherical harmonics Y_l^m. The most problematic ones are derivatives with respect to ϑ, where one of several recurrence relations for the Legendre polynomials should be used. One possible choice that comes without issues at the poles $\vartheta = 0, \pi$ is presented in reference [287]. Taking into account the Condon-Shortley phase and using the chain rule, we find

$$\frac{\partial}{\partial\vartheta} Y_l^m(\vartheta, \varphi) = -\frac{1}{2}\sqrt{(l+m)(l-m+1)}\, Y_l^{m-1}(\vartheta, \varphi) e^{i\varphi} + \frac{1}{2}\sqrt{(l-m)(l+m+1)}\, Y_l^{m+1}(\vartheta, \varphi) e^{-i\varphi}\,, \tag{B7a}$$

$$\begin{aligned}\frac{\partial^2}{\partial\vartheta^2} Y_l^m(\vartheta, \varphi) = {}& \frac{1}{4}\sqrt{(l+m)(l+m-1)(l-m+1)(l-m+2)}\, e^{2i\varphi} Y_l^{m-2}(\vartheta, \varphi) \\ & - \frac{1}{4}\big[(l-m+1)(l+m) + (l-m)(l+m+1)\big] Y_l^m(\vartheta, \varphi) \\ & + \frac{1}{4}\sqrt{(l-m)(l-m-1)(l+m+1)(l+m+2)}\, e^{-2i\varphi} Y_l^{m+2}(\vartheta, \varphi)\,.\end{aligned} \tag{B7b}$$

In eq. (B7a), the full Y_l^{m-1} term is missing for $m = -l$ and the full Y_l^{m+1} term is missing for $m = l$ (so the result is simply zero for $m = l = 0$). Similar for eq. (B7b), the term containing Y_l^{m-2} is absent for $m \leqslant -l+1$ and the full Y_l^{m+2} term must be omitted for $m \geqslant l-1$. Fortunately, φ derivatives are simpler: The k'th derivative is obviously given by

$$\frac{\partial^k}{\partial\varphi^k} Y_l^m(\vartheta, \varphi) = (im)^k Y_l^m(\vartheta, \varphi)\,, \quad k \in \mathbb{N}\,. \tag{B8}$$

We use these formulas to compute derivatives of f by substituting them into eq. (B6), e.g.

$$\frac{\partial}{\partial\vartheta} f(\vartheta_i, \varphi_j) \approx \sum_{l=0}^{p} \sum_{m=-l}^{l} \hat{f}_l^m \left[\frac{\partial}{\partial\vartheta} Y_l^m(\vartheta, \varphi)\right]\Big|_{\substack{\vartheta=\vartheta_i \\ \varphi=\varphi_j}}\,. \tag{B9}$$

We note that second order derivatives should not be computed by two successive first order derivatives involving one back and forward transformation, because not every first order derivative results in a smooth function on the surface. As an example take the z-component of the unit sphere, $z(\vartheta, \varphi) = \cos\vartheta$. Its first order derivative is $\partial_\vartheta z(\vartheta, \varphi) = -\sin\vartheta$, which is not smooth at $\vartheta = 0, \pi$ when considered on the sphere (compare e.g. $\varphi = 0$ and $\varphi = \pi$). Thus, its series expansion converges only very slowly. Direct computation of the second order derivative via eq. (B7b) circumvents this particular problem. The same holds for derivatives with respect to φ and mixed derivatives.

With this setup in place, calculating the traction jump from eq. (7) is more or less straightforward. We employ the definitions and results of differential geometry from sec. A 1 with $\theta^1 = \vartheta$ and $\theta^2 = \varphi$. However, for notational convenience we will use the alternative names

$$E := a_{11}\,, \quad F := a_{12} = a_{21}\,, \quad G := a_{22}\,, \tag{B10a}$$

$$L := b_{11}\,, \quad M := b_{12} = b_{21}\,, \quad N := b_{22}\,. \tag{B10b}$$

With $W^2 := EG - F^2$, the mean curvature is then given by [101]

$$H = \frac{EN - 2FM + GL}{2W^2} \tag{B11}$$

and the Gaussian curvature by

$$K = \frac{LN - M^2}{W^2}\,. \tag{B12}$$

The Laplace-Beltrami operator of some function f is [101]

$$\begin{aligned}\Delta_S f = {}& \frac{1}{W}\frac{\partial}{\partial\varphi}\left(\frac{E\partial_\varphi f - F\partial_\vartheta f}{W}\right) \\ & + \frac{1}{W}\frac{\partial}{\partial\vartheta}\left(\frac{G\partial_\vartheta f - F\partial_\varphi f}{W}\right)\,,\end{aligned} \tag{B13}$$

which in the present context is of course only really applied to H.

In practice, we start by computing the grid (ϑ_i, φ_j) for a given order p with $i = 0, \dots, p$ and $j = 0, \dots, 2p+1$ as explained above. The surface nodes $\boldsymbol{x}(\vartheta_i, \varphi_j)$ for the RBC shape are then obtained by setting [27]

$$x_1(\vartheta_i, \varphi_j) = R \sin\vartheta_i \cos\varphi_j \,, \tag{B14a}$$
$$x_2(\vartheta_i, \varphi_j) = R \sin\vartheta_i \sin\varphi_j \,, \tag{B14b}$$
$$x_3(\vartheta_i, \varphi_j) = \pm\frac{R}{2}\sqrt{1-\rho^2}(C_0 + C_1\rho^2 + C_2\rho^4) \,, \tag{B14c}$$

where R is the given length of the large half-axis, $\rho^2 := (x^2+y^2)/R^2$, $C_0 = 0.2072$, $C_1 = 2.0026$ and $C_2 = -1.1228$ [203, 378]. The plus sign is used for $\vartheta \leqslant \pi/2$, the minus sign otherwise.

Next, each individual Cartesian component of $\boldsymbol{x}$ is transformed via eq. (B5) to provide the representation in the spectral domain. First and second order derivatives (in the spatial domain) are then obtained by means of equations (B7a), (B7b) and (B8) in conjunction with backward transforms as in equation (B9). This allows us to calculate H and K at each grid point (ϑ_i, φ_j).

For $\Delta_S H$, eq. (B13) as well as W are first expanded by hand via the chain rule. Derivatives of E, F, G are obtained directly from the spectral coefficients of $\boldsymbol{x}$ as before. To get the derivatives of H, we first transform H into spectral space (eq. (B5)) and then apply again the derivative formulas (B7). Afterwards, the traction jump from eq. (7) is obtained by combining all temporary results.

We emphasize again that the transform (B5) is only applied to the components of $\boldsymbol{x}$ and once for H, but not to any other intermediate quantity such as $a_{\alpha\beta}$ or $b_{\alpha\beta}$. In principle, it would be possible to bypass the transform of H by expanding $\Delta_S H$ via the chain rule until only derivatives of $\boldsymbol{x}$ (up to fourth order) remain, which can then be evaluated directly using formulas similar to equation (B7a) [287]. We speculate that it would boost algorithmic precision because the only case where aliasing can then occur is in the transform of $\boldsymbol{x}$. This should make de-aliasing procedures as used in references [84, 101, 103, 207] obsolete. Considering the results presented in section III C, we would then expect a similar drop to machine precision for the traction jump in figure 4 as seen for the mean curvature in figure 3. However, deriving the necessary formulas is quite cumbersome and therefore has not been attempted so far.

On a related note, the de-aliasing rules mentioned in references [84, 101, 103, 207] are only required in the first place if other formulas need to be evaluated that are content with smaller orders of p. In this case, the smaller order can be upsampled by means of interpolation (i.e. evaluating eq. (B6) also at intermediary points) for the sake of computing the bending forces with a higher resolution.